frontiers in Energy Research

REVIEW
published: 28 May 2021
doi: 10.3389/fenrg.2021.625123

Physical Vapor Deposition of Cathode Materials for All Solid-State Li Ion Batteries: A Review

Berik Uzakbaiuly[1,2], Aliya Mukanova[1,2], Yongguang Zhang[3] and Zhumabay Bakenov[1,2,4]**

[1]National Laboratory Astana, Nazarbayev University, Nur-Sultan, Kazakhstan, [2]Department of Chemical and Materials Engineering, Nazarbayev University, Nur-Sultan, Kazakhstan, [3]Research Institute for Energy Equipment Materials, Hebei University of Technology, Tianjin, China, [4]Institute of Batteries LLC, Nur-Sultan, Kazakhstan

With the development of smart electronics, a wide range of techniques have been considered for efficient co-integration of micro devices and micro energy sources. Physical vapor deposition (PVD) by means of thermal evaporation, magnetron sputtering, ion-beam deposition, pulsed laser deposition, etc., is among the most promising techniques for such purposes. Layer-by-layer deposition of all solid-state thin-film batteries *via* PVD has led to many publications in the last two decades. In these batteries, active materials are homogeneous and usually binder free, which makes them more promising in terms of energy density than those prepared by the traditional powder slurry technique. This review provides a summary of the preparation of cathode materials by PVD for all solid-state thin-film batteries. Cathodes based on intercalation and conversion reaction, as well as properties of thin-film electrode–electrolyte interface, are discussed.

Keywords: thin-film batteries, cathode, Li ion batteries, physical vapor deposition, thermal evaporation

OPEN ACCESS

Edited by:
Chuan-Fu Lin,
The Catholic University of America, United States

Reviewed by:
Hui Xia,
Nanjing University of Science and Technology, China
Xia Li,
Concordia University, Canada

****Correspondence:***
Berik Uzakbaiuly
berik.uzakbaiuly@nu.edu.kz
Zhumabay Bakenov
zbakenov@nu.edu.kz

Specialty section:
This article was submitted to Electrochemical Energy Conversion and Storage, a section of the journal Frontiers in Energy Research

Received: *02 November 2020*
Accepted: *26 April 2021*
Published: *28 May 2021*

Citation:
Uzakbaiuly B, Mukanova A, Zhang Y and Bakenov Z (2021) Physical Vapor Deposition of Cathode Materials for All Solid-State Li Ion Batteries: A Review. Front. Energy Res. 9:625123. doi: 10.3389/fenrg.2021.625123

INTRODUCTION

As the world's population grows and environmental issues become more serious, it is important to find a safer, more reliable, and robust energy supply to replace conventional fossil fuels. Usage of renewable energies, such as solar energy, wind energy, ocean energy, or geothermal energy, is often limited by location and meteorological conditions, which is the reason why energy-storage solutions are needed to support the energy economy. The growing demands of electric vehicles and portable electronics have now significantly stimulated the development of energy storage devices such as lithium ion batteries (LIBs). For more than two decades, there has been tremendous research in the LIB field because of their high energy and power density. Several research groups have reported LIBs with energy densities greater than 500 Wh kg^{-1} (Liu et al., 2019; Park et al., 2019; Han et al., 2020; Qiao et al., 2020). Such batteries are based on liquid electrolytes (thickness ~25 μm due to the separator) and usually have electrode thicknesses in the order of ~50–60 μm (Singh et al., 2015). However, capacity retention issues and problems due to lithium dendrite growth and dead lithium which can cause severe safety problems have not been solved entirely to enable large-scale application. Solid-state lithium ion batteries are considered to be a solution for energy density of typical LIBs because they do not require a rigorous battery management system and the risk of thermal runaway is eliminated. Conventional solid-state batteries have electrolyte thicknesses in the order of ~20–100 μm (Wu et al., 2021). But, until now, the cyclability of solid-state cells has been limited mainly due to the electrode/electrolyte interfacial resistance and the volatility of solid electrolytes against lithium. For applications such as wearable and implantable devices, wireless

sensor networks, and Internet of Things, the drive toward miniaturized electronics calls for the production of micro energy storage systems that can allow continuous, autonomous operation of electronic devices. Owing to this, all solid-state thin-film batteries (ASTBs) featuring long lifetimes, high rate capabilities, and superior energy and power density are gaining attention because they are ideal candidates for integration into miniaturized energy systems. Full-stack ASTBs have thicknesses of only ~10–15 μm including current collectors, electrolyte, and electrodes, yet the substrate thickness at least doubles the overall battery thickness (Dudney 2008). Thin-film electrodes manufactured by physical vapor deposition (PVD), chemical vapor deposition (CVD), and atomic layer deposition (ALD) are recognized as pure materials since they do not have binders or conductive materials as in conventional powder slurry technology (Dasgupta et al., 2015; Kozen et al., 2015; Xie et al., 2017; Gandla and Tan 2019; Lidor-Shalev et al., 2019). However, large breakdowns in electrochemical efficiency are still noticeable for electrode components, electrolytes, and electrode–electrolyte interfaces.

Planar ASTBs suffer from the fact that the energy stored increases linearly with the thickness of the electrodes, and if the electrodes are too thick, Li ions (Li^+) will not diffuse to the whole depth of the electrodes. This can lead to lower capacity than expected for thick electrodes (Ohtsuka and Sakurai 2001). In addition, power density is compromised when higher thickness is coupled with slow Li^+ kinetics in the electrolyte. These drawbacks made researchers look into 3D electrodes and battery architectures for enhancing ASTB performance (i.e., increasing the capacity without sacrificing fast charging) (Oudenhoven et al., 2011; Bünting et al., 2015; Liu et al., 2018; Xue et al., 2019). Nevertheless, several groups have shown very promising works involving planar ASTBs, and there are several companies that produce commercialized 2D thin-film batteries such as Ilika, Cymbet, and STMicroelectronics (Dudney 2008; Chen et al., 2009; Larfaillou et al., 2016; Kyerematen and Hahn 2018).

Electrodes for ASTBs could be manufactured using several techniques such as PVD, CVD, and ALD. In a typical CVD chamber, the substrate is exposed to one or more volatile precursors that react to make the desired deposit on the top of the substrate and by-products are extracted *via* the gas flow through the reactor. CVD techniques have been used for growing nanostructured current collectors, active electrode materials, coatings, and for separator modifications (Wang and Yushin 2015). ALD, which is also a chemical method, involves exposing the surface of a substrate to alternating precursors, which are sequentially added and do not mix. It can be used to make atomically thin and uniform layers to enhance the performance of electrodes and make a 3D battery since it can cover nanocontours very uniformly (Liu et al., 2018). Although CVD and ALD are powerful techniques for deposition of high-quality cathode materials for batteries, they are still at an immature phase and currently the research-level systems are too costly. In addition, to fabricate a full planar battery, one may still resort to using PVD techniques. While each of the mentioned methods has their advantages and disadvantages, this work will mainly focus on physical vapor deposition of cathode electrodes for ASTBs.

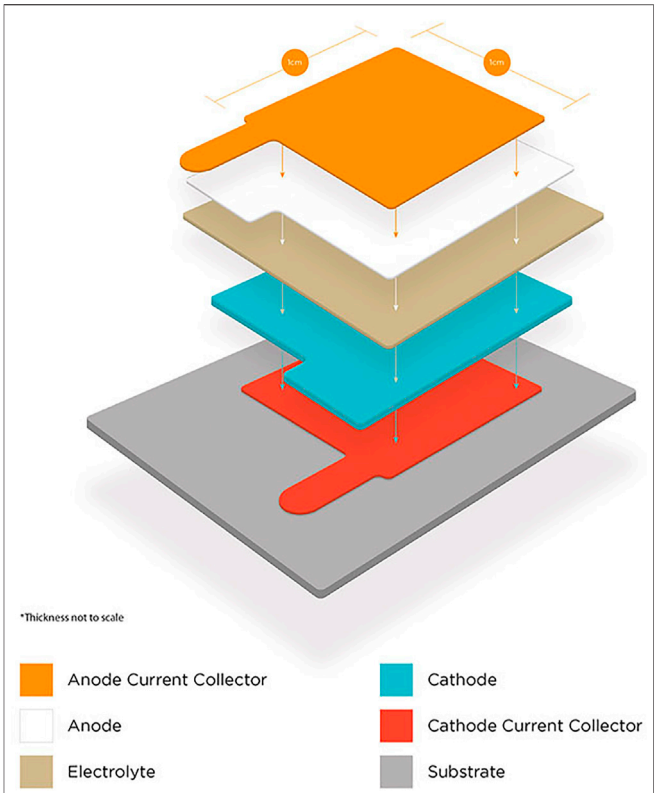

FIGURE 1 | Cell configuration of ASTBs combined with PVD methods. © Ilika Technologies.

Physical vapor deposition is a technique where materials are transferred from a condensed phase to a vapor phase and back to a condensed phase as a thin film on a substrate. It is a vacuum deposition method where several techniques could be used (**Figure 1**).

Thermal Evaporation

Thermal evaporation takes place in a vacuum by passing a large current through a resistive wire or boat which heats the source that it contains. As a result of low pressure and high temperature, the source material sublimes, gets deposited onto the substrate, and condenses as a thin film. Before this process, high vacuum should be achieved in the deposition chamber since it will increase the mean free path of the source material and allow vapor particles to travel directly to the substrate (**Figure 2A**). In the battery field, this method is mostly used to deposit lithium metal, which is usually deposited at thicknesses of 1 μm or more (**Supplementary Table S1**). As the lithium readily alloys with most of the materials, molybdenum or tantalum crucibles/boats are used in this method. Thermal evaporation has poor surface coverage and can cause some problems in controlling the thickness of the final thin-film material.

Sputter Deposition

This method requires the ejection of a "target" material from a source on a substrate. It happens in a plasma environment where

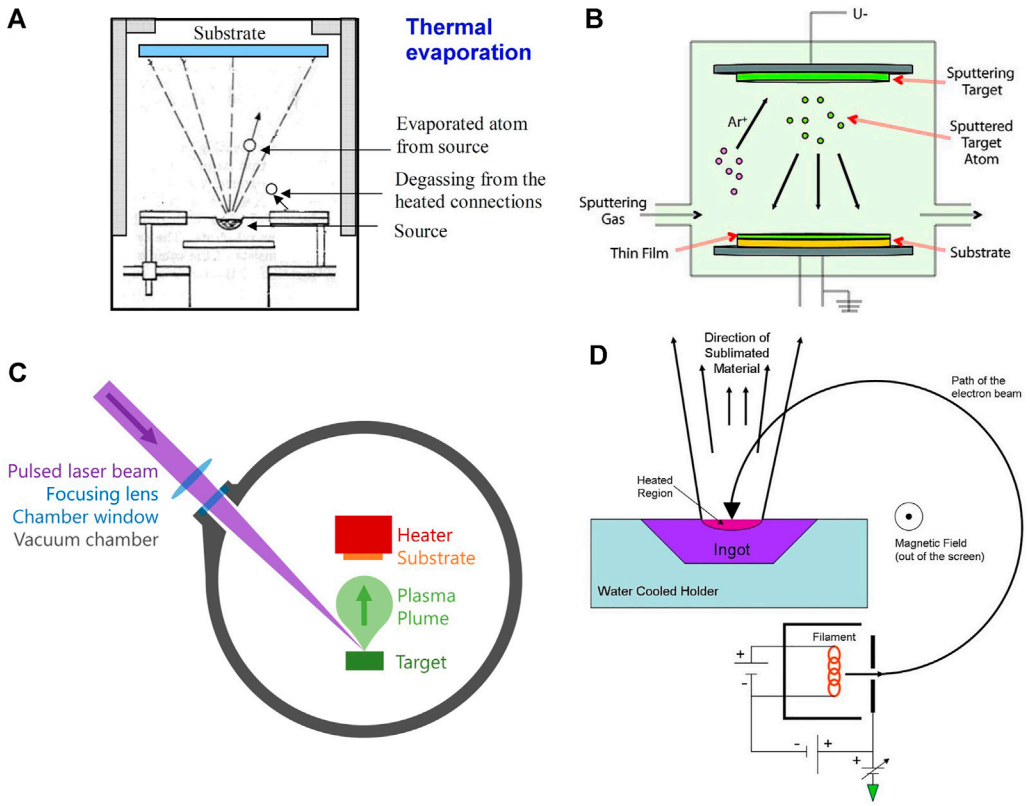

FIGURE 2 | Various physical vapor deposition techniques. **(A)** Thermal evaporation, S. Babar, CC BY-SA 3.0, *via* Wikimedia Commons, **(B)** sputter deposition using Ar gas, Sigma-Aldrich, CC BY-SA 4.0, *via* Wikimedia Commons, **(C)** pulsed laser deposition, **(D)** electron beam evaporation, Jatosado, CC BY-SA 3.0, *via* Wikimedia Commons.

ions are created from gasses such as argon, nitrogen, or oxygen. These ions bombard the target material and the target particles can fly out, travel toward the substrate, and deposit on it (**Figure 2B**). Several sputter deposition techniques exist, such as magnetron sputtering, reactive magnetron sputtering, ion beam sputtering, ion beam–assisted deposition, and high-power impulse magnetron sputtering.

Magnetron sputtering has been extensively used to deposit several cathode and anode materials for ASTBs. The most popular intercalation-based $LiCoO_2$ cathode is well studied under sputter deposition. However, most require post-annealing at 700°C to achieve high crystallinity since otherwise, the sputtered electrode will be amorphous and will not show good performance (Bates et al., 2000). Reactive magnetron sputtering is mostly used for deposition of electrolytes. In particular, lithium phosphorus oxynitride (with chemical structure $Li_xPO_yN_z$) (Lipon) electrolyte, which was developed at Oak Ridge National Laboratory (ORNL), remains one of the best electrolytes for lithium ion batteries since it is more stable in air than lithium oxide or sulfide-based batteries and shows very stable performance up to 5 V *vs* Li/Li^+ (Put et al., 2018). Radio frequency magnetron sputtering of a Li_3PO_4 target in a nitrogen environment is used to incorporate nitrogen in the final Lipon structure. Precise nitrogen incorporation in Lipon plays a key role in electrochemical stability and ionic conductivity in Lipon electrolytes. The experimental results along with the structural models showed that N forms both bridges between two phosphate units and nonbridging apical N in Lipon, and this appears to directly correlate with and explain both the increase in ionic conductivity and electrochemical stability (Lacivita et al., 2018).

Pulsed Laser Deposition

Pulsed laser deposition (PLD) is a method consisting of a high-power pulsed laser that is focused on the target material that is to be deposited. The target material gets vaporized into a plasma plume and deposits onto a substrate (**Figure 2C**). The process of etching is very complex because as the laser power gets absorbed by the target, many particles are ejected, such as electrons, atoms, ions, and clusters. Deposition efficiency depends on the type of target material, pulse energy of the laser, repetition rate, target substrate distance, substrate temperature, etc. PLD may be used to ablate many materials and combinations by selecting the appropriate laser wavelength to match the absorption properties of the target. There are many works that used PLD to fabricate one component of a battery (electrode, electrode coatings, or electrolyte) for application in ASTBs (Yamada et al., 2003; Park et al., 2006; Yamada et al., 2007; Saccoccio et al., 2017;

TABLE 1 | Summary of the advantages and disadvantages of PVD methods.

Methods	Sources	Advantage	Disadvantage
Thermal evaporation	Metal or low melting point materials	•Low cost •High-purity films	•Cannot evaporate refractory materials •Poor uniformity
Sputtering	Ceramics or metals	•High growth rate •Large area	•Damage by ionized particle •Elemental selective supply rate
Pulsed laser deposition	Ceramics, metals, or single crystals	•Stoichiometric transfer •Wide applicability	•Low growth rate •Spontaneous defect formation
E-beam evaporation	Ceramics or metals	•Suitable for high melting point metals •Little contamination	•Energetic electrons may damage films •Limited step coverage

Teng et al., 2018; Yu et al., 2018; Fenech and Sharma 2020). However, only few have actually fabricated ASTBs with thin-film solid electrolytes using PLD techniques (Huang et al., 2003; Huang et al., 2004; Kuwata et al., 2004; Baskaran et al., 2009; Matsuda et al., 2018).

Electron Beam Deposition

This method comprises a charged tungsten filament from which electron beams are accelerated and bombard the target material (**Figure 2D**). The electron beam converts atoms from the target into the gas phase and the atoms then flow toward the substrate, precipitate into the substrate, and create a thin-film layer. With e-beam deposition, one can get a deposition rate of 0.1–100 μm min^{-1}, which is higher than that using conventional PVD processes. However, just as in the PLD method, very few works have shown ASTBs which utilized the e-beam evaporation technique (Huang et al., 2004; Li et al., 2006a; Schwenzel et al., 2006). **Table 1** lists the advantages and disadvantages of the PVD methods for the fabrication of ASTBs.

In this review, we will first focus on cathode materials based on lithium transition metal oxides, then metal oxides, then lithium phosphates, and finally touch upon sulfide and tungstate materials. Afterward, we will discuss the interfacial properties between cathodes and electrolytes of ASTBs. The readers are advised to refer to **Supplementary Table S1** throughout the discussion.

DISCUSSION

Lithium Transition Metal Oxide Cathodes

$LiCoO_2$ With Lipon Solid-State Electrolyte

Since the discovery of the Lipon electrolyte (by the group at ORNL) which had increased conductivity and increased stability toward lithium (Li) (Bates et al., 1992), research in thin-film batteries has been booming. $LiCoO_2$ is the most studied cathode material used with Lipon solid electrolyte. Bates et al. have laid out several thin-film batteries and the crystalline $LiCoO_2$/Lipon/Li battery is the most mature with the highest capacity, energy, and power densities (Bates J. et al., 2000). The cell showed a capacity of 64 μAh cm^{-2} $μm^{-1}$, which is close to the theoretical capacity of 69 μAh cm^{-2} $μm^{-1}$ or 137 mAh g^{-1} at $Li_{0.5}CoO_2$ extraction of Li. The cell showed a capacity of 62 μAh cm^{-2} $μm^{-1}$ at 4000 cycles, and shelf lives are estimated for many years by looking at open circuit voltage. Post-annealing at 700°C is required for these samples to obtain the highest capacity. It has also been shown by the ORNL group that $LiCoO_2$ has preferential orientation upon thickness. Less thick $LiCoO_2$ (<1 μm) showed (003)-oriented grains parallel to the substrate, while thicker films (>1 μm) had their (101) and (104) planes parallel to the substrate as confirmed by X-ray diffraction (XRD) and electron microscope measurements (SEM and TEM) (Bates et al., 2000). Jang et al. fabricated $LiCoO_2$ using sputtering techniques and post-annealed at 800°C in O_2 instead of the usual 700°C for the material. The battery ($LiCoO_2$/Lipon/Li ASTB) was cycled up to 4.4 V, and a capacity of 170 mAh g^{-1} (~85.6 μAh cm^{-2} $μm^{-1}$) at a current density of 100 μA cm^{-2} was observed, which is 22% higher than that reported by previous reports (Jang et al., 2003). $LiCoO_2$ had nanocrystalline grain structures as observed by TEM, and the excellent cyclability of the thin-film batteries is attributed to the small grain size of the cathode film and the stability of the Lipon electrolyte.

Since Li metal is not compatible for solder reflow processing of microelectronic devices, the ORNL group fabricated "Li-free" thin-film batteries, where upon first charge, Li was plated on a Cu anode (Bates J. et al., 2000). The key to having good cycle stability is protecting Cu and covering with an overlayer consisting of electron and Li^+ blocking parylene, over which Ti was deposited to reduce air permeability. Without the overlayer, capacity dropped by 45% and blossom-like features appeared between Lipon and Cu. It is believed that the Li^+ penetrates through the Cu anode, reacts with even the small amount of air present between the overlayer and Cu, and forms a passivation layer of LiO_2 or LiOH. Cycle performance of Lipon overlayer battery and parylene + Ti overlayer battery was compared over 1000 cycles at 1 mA cm^{-2}, and parylene + Ti showed batter capacity retention. SEM cross-sectional pictures of Lipon and parylene + Ti overlayer clearly showed the latter's favorable property. The Li-free thin-film battery survived solder reflow conditions, which were simulated as rapid heating to 250°C for 10 min and rapid quenching with air. Other groups that showed "Li-free" technology with Lipon electrolyte have used different types of anodes. D. Li et al. made a $LiCoO_2$/Lipon/SnN thin-film battery and checked the temperature performance from 20 to 200°C because Li cannot withstand those temperatures (Li et al., 2014). The results showed that the thin-film battery maintains a good high-temperature discharge performance before 100°C after which its capacity was lower than that for the ambient. No specific capacity was given, so the capacity of an ~188-μAh cell was stable at 100°C for 15 cycles. Also, Gong et al.

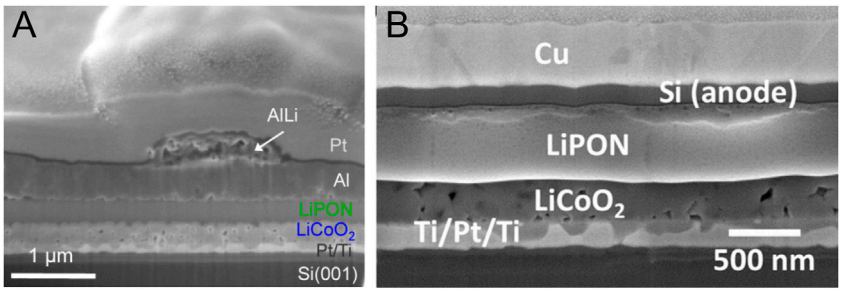

FIGURE 3 | (A) Cross-sectional SEM image of Al electrode after 10 charging cycles, tilt = 45°. The Pt layer is added uniquely to protect the surface of the battery during the ion milling process and is not an active layer of the device. Reprinted with permission from Gong et al. (2015). © 2015 ACS **(B)** Focused ion beam cross section of an ASTB. Reprinted with permission from Talin et al. (2016). © 2016 ACS.

fabricated a $LiCoO_2$/Lipon battery with 400 nm Al, 400 nm Al/400 nm Cu, and 50 nm Si/400 nm Cu-negative electrodes (Gong et al., 2015). With Al anode, ASTBs showed a very rapid capacity decay, which was accompanied by volume expansion of the negative electrode. ~1 μm diameter mounds of AlLi alloy were formed on the surface of ASTBs (**Figure 3A**). X-ray photoelectron spectroscopy (XPS) measurements showed Al-Li-O compounds formed on the top of the Al electrode, which increased electrical resistance and hence degraded the battery's overall performance. Capping the Al electrode with Cu did not resolve the rapid capacity loss, if not worsened it. Nonetheless, ASTBs with Si-negative electrodes capped with Cu exhibit remarkably stable performance, retaining >92% of their discharge capacity after 100 cycles. Since Li^+ diffuses almost 10 orders of magnitude faster in Si than it does in Al, the surface mounds and the associated trapped Li are not observed and an insulating compound of Si–O–Li does not seem to form on the Si electrode surface. It has also been shown that a $LiCoO_2$/Lipon/Si ASTB showed significantly higher power performance than a 3D counterpart (**Figure 3B**) (Talin et al., 2016). This is attributed to low electrolyte ionic conductivity and poor homogeneity which lead to a highly nonuniform internal current density distribution and poor cathode utilization.

To decrease the post-annealing step at 700°C, bias sputtering of the cathodes, where the substrates were biased under a negative voltage, has also been studied by several groups. Park et al. fabricated ASTBs with bias-sputtered $LiCoO_2$ (Park et al., 2005). Sputtered and annealed samples are found to be well crystallized but have micro-cracks and voids due to the difference in thermal expansion of $LiCoO_2$ and Ti/Pt-coated Si wafer. Charge discharge tests also showed a linear decrease in specific capacity, starting at 59 μAh cm^{-2} μm^{-1} and ending at 32 μAh cm^{-2} μm^{-1} at 100 cycles. ASTBs with cathode bias sputtered at −50 V showed more stable performance, and the discharge capacity was ~63 μAh cm^{-2} μm^{-1} and after 100 cycles remained around 52 μAh cm^{-2} μm^{-1}. From the XRD patterns, the structure of the cathode is amorphous, yet there are some randomly oriented crystalline grains in the bulk of the thin film as observed by TEM. It is supposed that the substrate bias changes the crystal structure and orientation through the ion bombardment that occurs when inducing bias. Navone et al. made ASTBs with $LiCoO_2$ cathode which was sputtered at a bias of −50 V and post-annealed at 500°C (Navone et al., 2011). Thin cathode film of 0.45 μm was tested at high C rates. Kinetic properties revealed a capacity of 42 μAh cm^{-2} μm^{-1} at 30°C (~750 μA cm^{-2}) without damaging the film electrode, and yet a capacity of 50 μAh cm^{-2} μm^{-1} can be recovered at the 0.4°C (~10 μA cm^{-2}) rate. The capacity of the ASTB dropped from 55 μAh cm^{-2} μm^{-1} to 50 μAh cm^{-2} μm^{-1} when cycled at 10 μA cm^{-2} for 140 cycles. Later, the same group looked at the capability rate of the above bias-sputtered cathodes (Tintignac et al., 2014). They found that battery performance is worse when charged at high currents and discharged at low currents, than when charged at low currents and discharged at high currents. At higher charge cut-off voltages (4.5 V), ASTBs also behave poorly. This phenomenon is ascribed to the occurrence of irreversible structural and volume changes when the depth of charge is too high. Discharging at 10 μA cm^{-2} current density for 900 cycles showed the following trend: After an initial capacity fade by 8% over the first 100 cycles, the capacity slowly declined over 800 additional cycles to reach 40 μAh cm^{-2} μm^{-1} at the end. The capacity loss per cycle is limited to 0.005% from cycle 100 to cycle 900.

Alternatively to post-annealing at high temperatures, rapid thermal annealing (RTA) was utilized to fabricate ASTBs on a flexible substrate (Song et al., 2010). $LiCoO_2$ was sputtered and was put through RTA at 520°C for 15 min so as to not damage the mica substrate. Cells without encapsulation and those with multilayered encapsulation for which the exterior of the ASTB was alternately coated, layer by layer, 3–4 times with polymeric and oxide films using CVD and sputtering were studied at high C rates. Without encapsulation, reduced normal orientation of columnar grains and aggregation of the grains are observed. In contrast, for cells with encapsulation, not only the original morphology of the $LiCoO_2$ columnar grains but also the smooth interfaces between the layers were sustained. Encapsulated ASTBs at 10°C show excellent capacity retention of 95% over 800 cycles, delivering >22 μAh cm^{-2} μm^{-1}. Another group that achieved flexible batteries on PDMS substrate was Koo et al. (2012). $LiCoO_2$/Lipon/Li ASTBs had a capacity of ~30 μAh cm^{-2} μm^{-1}, which is lower than that for batteries on solid

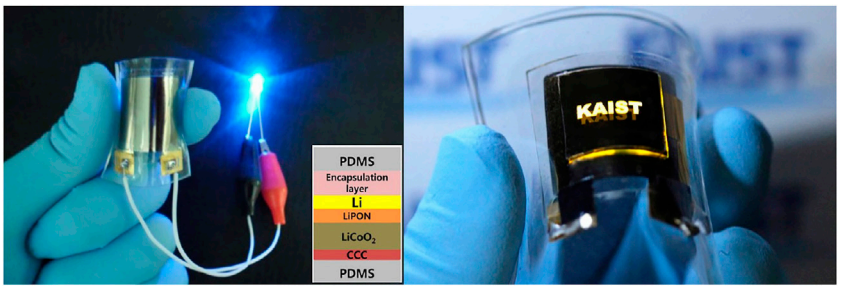

FIGURE 4 | Photograph of a bendable LIB turning on a blue LED in bent condition. The inset shows the stacked layers in the flexible LIB and the picture of an all-in-one flexible LED system integrated with a bendable LIB. Reprinted with permission from Koo et al. (2012). © 2012 ACS.

substrate. However, with an energy density of 2.2×10^3 μWh cm^{-3}, at 46.5 μA cm^{-2} (0.5°C) under polymer sheet wrapping, the battery could power a flexible LED system (**Figure 4**). Interestingly, specific capacity is different on a mica substrate and on a PDMS substrate. The authors claim that stresses induced on sputtered films on a mica substrate are gradually released upon delamination of the mica layers, and when transferred to a PDMS substrate, the battery performs better. Thus, the capacities of LIBs transferred onto polymer substrates can be increased due to the prompt release of stresses by the molar volume change. The flexible battery has a specific capacity of 106 μAh cm^{-2} for the nonbending case, and for the bending case, at an effective radius of 3.1 mm, the specific capacity decreased to 99 μAh cm^{-2}.

In addition to sputtering, PLD has also been used to fabricate ASTBs with $LiCoO_2$ cathode. Matsuda et al. fabricated thin-film $LiCoO_2$ at high rate deposition of ~2–3 μm h^{-1} (Matsuda et al., 2018). Using high-power ArF laser, ASTBs with 0.3- to 30-μm–thick $LiCoO_2$ cathodes were constructed with amorphous Li_3PO_4 electrolyte. Highly crystalline cathodes were obtained as confirmed by XRD measurements. A buffer layer of $LiCoO_2$ was deposited on the substrate with low-frequency PLD, since otherwise thick (>1 μm) $LiCoO_2$ would exfoliate from the substrate after electrolyte deposition. With thick cathodes, the increase in C rate increases the interfacial resistance and Li^+ diffusion is limited to the surface. The maximum discharge capacities that were observed at a low current density of 10 μA cm^{-2} are 18 μAh cm^{-2} (for 0.32-μm–thick cathode), 100 μAh cm^{-2} (for 2.2-μm–thick cathode), and 240 μAh cm^{-2} (for 6.7-μm–thick cathode). These are 84%, 64%, and 54% of the theoretical capacity of $LiCoO_2$, which is 69 μAh cm^{-2} μm^{-1}. Theoretical calculations revealed that when the diffusion coefficient of Li^+ is low (10^{-12} cm^2/s), the capacity dependence flattens out and no longer increases with the increase in thickness. But for higher diffusion coefficients of Li^+ in cathode (10^{-11} cm^2/s), the capacity of ASTBs does increase with higher thickness. This was confirmed using potentiostatic intermittent titration technique (PITT) and electrochemical impedance spectroscopy (EIS) measurements. As the discharge progresses, the Li concentration near the surface of the Li_xCoO_2 increases and the chemical diffusion coefficient decreases. In this case, only the surface of the Li_xCoO_2 can be utilized and utilization of the thick $LiCoO_2$ film decreases. This was also confirmed by observing a crack formation near the interface of the cathode/electrolyte.

$LiCoO_2$ With Other Solid-State Electrolytes

Earlier, sequential PLD was used to fabricate ASTBs with amorphous $Li_{2.2}V_{0.54}Si_{0.46}O_{3.4}$ (LVSO) solid electrolyte, crystalline $LiCoO_2$ cathode, and amorphous SnO anode (Kuwata et al., 2006). The solid electrolyte $Li_{2.2}V_{0.54}Si_{0.46}O_{3.4}$ was prepared by the solid-state reaction method from Li_2CO_3, SiO_2, and V_2O_5 powders. Comparing the Arrhenius plots of bulk and thin-film solid electrolytes, one clearly observes better performance for the former. The battery was cycled between 2.7 and 3.3 V and with very small current. The battery delivered a poor specific capacity of 22.5 μAh cm^{-2} μm^{-1} (9 μAh cm^{-2} with a cathode thickness of 400 nm) and was cycled till 100 cycles.

Related to this, other types of electrolytes were assembled with $LiCoO_2$ cathode (Lee et al., 2003). Lee et al. fabricated an electrolyte and tested its performance in a thin-film configuration. A battery with a $LiCoO_2$-positive electrode, a $Li_{1.9}Si_{0.28}P_{1.0}O_{1.1}N_{1.0}$ electrolyte, and a $Si_{0.7}V_{0.3}$-negative electrode was deposited sequentially solely by PLD. The electrolyte was obtained through sputtering of $0{:}8Li_3PO_4{*}0{:}2Li_2SiO_3$ in a N_2 environment and exhibited an amorphous structure with an ionic conductivity of 8.8×10^{-6} S cm^{-2}. The ASTB was tested and revealed very stable cycling up until 1500 cycles with a 2–3.9 V voltage range. Capacity fading of the battery when it was cycled between 2 and 3.9 V voltage range was much less than that with 2–4.2 V. It is speculated that $LiCoO_2$ is stable until 4.2 V with Li but not with Si. With Si, the cathode might be at a potential of 4.4–4.6 V if the battery itself is at 4.2 V. Yoon et al. fabricated LiBPON electrolyte by co-sputtering of Li_3PO_4 and Li_3BO_4 targets, and found a maximum ionic conductivity of 6.88×10^{-7} S cm^{-1}, at 50 W/20 W target powers, respectively (Yoon et al., 2013). Using a variety of characterization techniques such as inductive coupled plasma–auger electron spectroscopy (ICP-AES), XPS, Fourier transform infrared (FTIR) spectroscopy, and Raman spectroscopy, the formation mechanism in a new electrolyte was suggested. The formation of B-N=P in the glass network implicates the reduction of mobile lithium sites. On the contrary, the three-coordinated nitrogen (B-N < P) preserves or increases the number of mobile lithium sites by nonbridging P=O bonding. In addition, looking at the impedance plots, no severe

chemical reactions were found for samples exposed to air for 40 days. Yet, ASTBs showed a moderate specific capacity of 33 μAh cm^{-2} μm^{-1} at 15 cycles. In addition, Song et al. fabricated a flexible $LiCoO_2$/LiBON/Li thin-film battery on mica substrate by multilayer polymer/oxide encapsulation (Song, Lee, and Park 2016). This cell which had an area of ~3 cm^2 and a total thickness of ~10 μm (49.2 μAh cm^{-2} μm^{-1}) could fit into a credit card. Charge discharge characteristics showed 90% capacity retention for 1000 cycles. ICP-AES was performed to show a $Li_{3.09}BO_{2.53}N_{0.52}$ composition. FTIR and XPS measurements proposed that Li^+ ions transport through the ionic bonds of -B-(O/N)-. . .Li^+. Twist and bending experiments revealed 99%, low-temperature (−10°C) characterization revealed 77%, and high-temperature (60°C) characterization revealed 127% initial capacity. Moreover, a Li-rich Lipon electrolyte was assembled with a LCO cathode and showed better performance than a regular Lipon electrolyte (Xiao et al., 2018). Upon electrolyte deposition on a $LiCoO_2$ electrode, the cathode surface gets damaged by N_2 plasma and defects on the top of $LiCoO_2$ are induced, which in turn creates a space charge layer that later hinders Li ion diffusion. And to offset this, a Li-rich electrolyte was made that had a better rate capability over 26 cycles than normal Lipon.

$LiNiO_2$

HK Kim et al. fabricated a $LiNiO_2$/Lipon/Li battery using sputtering techniques and thermal evaporation (Kim et al., 2002). After sputtering, the cathode material was put through RTA for 10 min at 700°C, which is much faster than conventional slow annealing techniques. From the SEM cross-sectional view, it is seen that a small layer appeared that is believed to be the Li-O layer for as-deposited samples, and this layer was removed by the RTA process. This battery exhibited 57 μAh cm^{-2} μm^{-1} capacity and showed stable performance for 120 cycles. In addition, an ASTB with a $LiNi_{1-x}Co_xO_2$ cathode was made by the same group (Kim H. K. et al., 2002; Kim et al., 2004). An oxygen layer was formed on the top of the cathode when it was exposed to ambient temperatures. After RTA at 700°C for 5 min, this oxide layer was eliminated and the sample could cycle at a capacity of 60.2 μAh cm^{-2} μm^{-1} for 100 cycles. AES did confirm that the content of the surface layer was Li-O.

$LiMn_2O_4$ and $Li_2Mn_2O_4$

This spinel-type cathode material was also studied thoroughly by research groups. Manganese-deficient–lithium-rich samples were obtained ($Li_{1+x}Mn_{2-y}O_4$) upon sputtering of $LiMn_2O_4$, and it had several discharge plateaus at 5 V, 3.8 V, and sometimes 4.6 V (Bates et al., 1995). Models to account for 5 V plateau are based on partially inverse spinel structures with some Mn^{4+} ions on the 8a sites and Li^+ ions on 16d sites. The capacity for 0.6 Li per Mn_2O_4 at 4 V is confirmed experimentally based on extracted charge and mass of cathodes (Bates et al., 2000). Park et al. (1999) made an ASTB with $LiMn_2O_4$ cathode. A battery with a small active area of >2.5 mm^2 and thickness of 300 nm showed a capacity of 48 μAh cm^{-2} μm^{-1}, which is 80% capacity of $LiMn_2O_4$ (0.8 Li per mole of Mn_2O_4). The rate capability is impressive: The discharge capacity obtained at 800 μA cm^{-2} was about 45 μAh cm^{-2} μm^{-1}, which represents more than 90% of the capacity obtained at lower currents. This indicates fast lithium intercalation kinetics within the $LiMn_2O_4$ spinel structure and a small ohmic drop across the solid electrolyte. Another group has also fabricated ASTBs with lithium anode (Li and Fu 2007). As with previous observations, $LiMn_2O_4$ has two distinct plateaus at 4 and 3 V regions during the charge/discharge process. XRD showed the amorphous structure of the films, but TEM diffraction patterns showed polycrystalline stripes in the bulk of $LiMn_2O_4$. The discharge capacity of the cathode is maintained at 78 μAh cm^{-2} μm^{-1} within 300 cycles. EIS measurements revealed that Li diffusion is about 8.7×10^{-11} cm^2 s^{-1}. Moreover, Xia et al. fabricated a 3D structured $LiMn_2O_4$ cathode with Lipon electrolyte and Li anode (Xia et al., 2018). The target was $Li_{1.15}Mn_2O_4$ and had excess Li content to compensate for the Li loss during sputtering. The 3D $LiMn_2O_4$/Lipon/Li ASTB had an initial capacity of 24.2 μAh cm^{-2} and showed 90% capacity retention after 500 cycles at 1°C, while the capacity retentions of 2D counterparts were ≤73%. Later, the same group fabricated 3D tunnel intergrowth Li_xMnO_2 nanosheet arrays using low-temperature processing (180°C) with the assistance of electrolyte Li^+ ion infusion (Xia et al., 2020). The Li_xMnO_2/LiPON/Li ASTB showed an initial capacity of 32.8 μAh cm^{-2} at a current density of 20 μAh cm^{-2} and retained 81.3% after 1000 cycles. These works show the significance of nanostructuring of cathodes for ASTBs.

Besides the Li anode, $LiMn_2O_4$ has also been tested with a V_2O_5-negative electrode in ASTBs (Baba et al., 2001). Interestingly, the initial capacity builds up to about 9 μAh cm^{-2} upon cycling. Upon exposure to air, the capacity does not degrade since the battery is "Li free." The latter group has also shown properties of $Li_2Mn_2O_4$ with various anodes such as V_2O_5 (Nakazawa et al., 2005), NbO (Nakazawa et al., 2007), and $Li_4Ti_5O_{12}$ (Nakazawa et al., 2015) by fabricating ASTBs with a large effective area of ~10 cm^2. During sputtering, some of the Li flies away and the final cathode becomes Li deficient, that is, $Li_{2-x}Mn_2O_4$. Reversible capacities of 18 μAh cm^{-2} μm^{-1} (100 cycles), 37 μAh cm^{-2} μm^{-1} (500 cycles), and 52 μAh cm^{-2} μm^{-1} (12,000 cycles) were obtained for ASTBs with V_2O_5, NbO, and $Li_4Ti_5O_{12}$ anodes, respectively. The voltage profile is linear from 0.3 to 3.5 V for ASTBs with V_2O_5 anode, and the battery exhibited a decrease in capacity during the first 10 cycles. ASTBs with NbO anode at various thicknesses of 50, 100, 200, and 300 nm were tested. Capacity based on the volume of both positive and negative electrodes for a 100-nm anode showed better performance than others. The ASTB with $Li_4Ti_5O_{12}$ anode shows an S-like voltage plateau, and this changes to a two-step shape upon anode thickness increase. TEM images of the cross section of the ASTB were investigated after 100 cycles. Each battery layer is condensed, nonporous before and after cycling, and the thickness of each layer that has a sharp and transparent interface resembles the initial thickness.

Doped Lithium Transition Metal Oxide Cathodes

A great deal of research has been undertaken on powder manufacturing of doped lithium transition metal cathodes, and thin-film batteries are no different. Whitacre et al. studied

$Li_yMn_xNi_{2-x}O_4$ cathodes where the x and y values varied between 0.2–1.8 and 2.7–3.7, respectively (Whitacre et al., 2003). Combinatorial sputtering of $LiMn_2O_4$ and $LiNiO_2$ targets revealed 590 μm × 590 μm sized ASTBs with different cathode compositions. The highest capacity observed was 115 mAh g^{-1} [~50.4 μAh cm^{-2} $μm^{-1}$ based on a density of 4.38 g cm^{-3} from Materials Project (Jain et al., 2013)] for a $LiMn_{1.35}Ni_{0.65}O_4$ cathode. This cathode showed the highest discharge plateau at 4.7 V among the other compositions. Proper substitution of Ni enables the production of thin-film cubic spinel cathodes with higher capacities and power densities than those reported for thin films of pure $LiMn_2O_4$. High-voltage thin-film cathodes of $Li_2MMn_3O_8$ (M = Fe, Co) were prepared by e-beam evaporation of targets that were added excess $LiNO_3$ (20 wt%) to compensate for Li loss during sputtering and to eliminate Mn_2O_3 impurity in the final films (Schwenzel et al., 2006). ASTBs could be operated between 3 and 5 V vs. Al, LiAl and showed a capacity of 42 μAh cm^{-2} $μm^{-1}$ and 33 μAh cm^{-2} $μm^{-1}$ for $Li_2CoMn_3O_8$ and $Li_2FeMn_3O_8$ cathodes, respectively. Chemical diffusion coefficients for the samples were in the range between $10^{-}13$ and 10^{-12} cm^2 s^{-1}, which is about three orders of magnitude lower than those of Li $(M_{1/6}Mn_{11/6})O_4$ [M = Mn, Co, (Co, Al)].

Doping was also carried out by incorporating mass quantities of ZrO_2 into $LiMn_2O_4$ for ASTBs (Li and Fu 2007). SEM images had no apparent grain boundary in the cathode film, which is attributed to ZrO_2 penetration in the $LiMn_2O_4$ film. Despite the removal of the two-step plateau structure in the voltage profile, the newly fabricated cathodes had a less volumetric capacity of 53 μAh cm^{-2} $μm^{-1}$ within 300 cycles. Since Zr is electrochemically inactive, EIS results confirmed a higher charge transfer resistance in the sample than that in a pure $LiMn_2O_4$ film. This group also demonstrated that ASTBs with $LiCoO_2$ cathode doped with Ni and Zr had different effects on the structural and electrochemical properties (Li et al., 2006). The target material for sputtering was made by solid-state reaction of powders, and thin films became crystalline after annealing at 700°C, which is also confirmed by SEM. For the XRD pattern of both films, preferential growth along the 003 plane was seen as films tend to minimize surface energy for thicknesses below 1 μm. Both films showed a layered structure, and upon Ni (electrochemically active) doping, the capacity increases relative to $LiCoO_2$, and upon Zr (electrochemically inactive) doping, higher nominal voltage and cyclic retention are observed. Baskaran et al. (2009) fabricated a $LiNi_{0.8}Co_{0.2}O_2$/$Li_{3.4}V_{0.6}Si_{0.4}O_4$/SnO battery solely using PLD. Post-annealing at various temperatures revealed random variation of Li content in the films since Li is an easily evaporable element and the stoichiometry of Li depends upon many parameters such as laser power, oxygen flow rate, and post-annealing temperatures. Cathode material annealed at 500°C showed best capacity (69.6 μAh cm^{-2} $μm^{-1}$) with one red-ox peak with liquid electrolyte. However, this is not comparable with the theoretical specific capacity of 136 μAh cm^{-2} $μm^{-1}$ for total extraction Li^+ from the host matrix of $LiNi_{0.8}Co_{0.2}O_2$. A severe drop in capacity is observed for $LiNi_xCo_{1-x}O_2$ thin films grown by RF magnetron sputtering due to the nonhomogeneity and nonstoichiometry of the films. Furthermore, the ASTB had only ~20 μAh cm^{-2} $μm^{-1}$ in the first cycles. Therefore, other compositions with mixed doping mechanism were investigated by research groups.

A target made out of $LiNi_{1/3}Mn_{1/3}Co_{1/3}O_2$ (NMC 111) powders was used to sputter cathodes for ASTBs (Ding et al., 2010). Thin cathodes (~0.15 μm) had a structure of $LiNi_{1/4}Mn_{1/2}Co_{1/3}O_2$ as claimed by XRD and EDS measurements. By looking at cyclic voltammetry (CV) redox peaks and plotting it vs. the square root of the scan rate, Li diffusion constants of 1.62×10^{-13}/1.78×10^{-13} cm^2 s^{-1} for Li^+ deinsertion/insertion processes were found. The ASTB was cycled up to 90 cycles and the capacity on the first cycles was 10.4 μAh cm^{-2} $μm^{-1}$, which then subsequently increased to reach a capacity of 33 μAh cm^{-2} $μm^{-1}$. This was attributed to the fact that the electrode–electrolyte interface became more convenient because polarization in the voltage profile was less with cycling. Interestingly, cathode film had a decreasing specific capacity upon cycling with liquid electrolyte. Another group also tried to fabricate ASTBs with NMC 111 cathode by sputtering (Feng et al., 2014). Polarization of the thin film in liquid electrolyte was high due to the relatively poor conductivity and showed two discharge plateaus after 10 charge/discharge cycles. The 2 V NMC/Lipon/TiO_2 microbattery delivered a specific capacity of 52 μAh cm^{-2} $μm^{-1}$ and 90% capacity retention after 400 cycles. Tan et al. prepared Li–Co–Ni–Mn oxide cathode thin films using powders of NMC 111 with excess of 10 mol% Li_2CO_3 to compensate for Li loss (Tan et al., 2014). The thin films were post-annealed at different temperatures and characterized using several techniques. XRD and Raman patterns indicated that 400°C post-annealed cathode displays a partially crystalline structure with (104) preferred orientation and that of 700°C exhibits crystallographic planes with (101) and (110) preferred orientations similar to those of the NMC 111 target. The AES depth profile showed a surface layer composed of Li, C, and O for the as-deposited sample, indicating reaction of the surface with air, and this layer was inhibited by post-annealing at higher temperatures. ASTBs with Li–Al–Ti–P–O–N solid electrolyte showed a specific capacity of 154.2 mAh g^{-1} (~69.4 μAh cm^{-2} $μm^{-1}$) and 127.2 mAh g^{-1} (~57.2 μAh cm^{-2} $μm^{-1}$) after 100 cycles. The impedance decreased until the fifth cycle and then increased with further cycling. It is assumed that the cyclability of the ASTB cell is strongly dependent on the interfacial stability between the cathode and the solid electrolyte. Remarkable cycle performance of ASTBs with $LiNi_{0.5}Mn_{1.5}O_4$ cathode was reported by the group at ORNL (Li et al., 2015). The first cycle irreversible charge capacity is mostly caused by the redox couple Mn^{3+}/Mn^{4+} instead of electrolyte decomposition, evidenced by the fact that the capacity of the 4 V plateau (≈40 mAh g^{-1}) equals the first cycle irreversible capacity. The excess lithium on the top of the cathode is eliminated during the first charge phase as well. Owing to its decreased electrolyte thickness, strong interfacial stability, and the rapid kinetics of the electrodes, the ASTB provides good rate capability. However, the active loading of the cathode is still low at 0.5 mg cm^{-2}, approximately 10 times smaller than in industrial batteries with liquid electrolyte. The reversible capacity under the C/10 rate is 122 mAh g^{-1} (~53.4 μAh cm^{-2} $μm^{-1}$) over 10,000 cycles, and upon increase in current density, the utilization

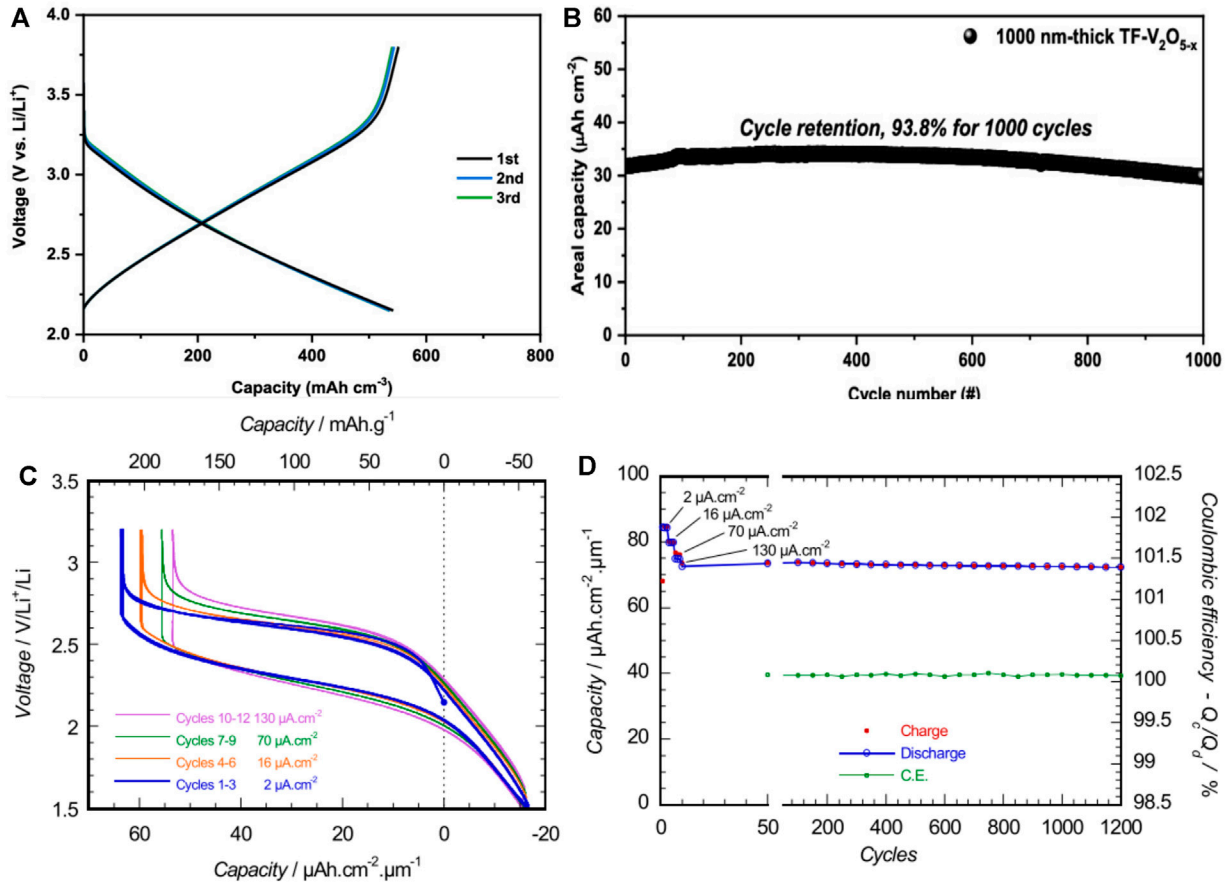

FIGURE 5 | (A) Galvanostatic discharge–charge profile of V_2O_{5-x}/Lipon/Al_2O_3 (1 nm)/Li ASTB and **(B)** long-term stability data of the cell at 2°C. Reprinted with permission from Xiao et al. (2021). © 2021 ACS. Galvanostatic cycling of **(C)** $Li_{1.2}TiO_{0.5}S_{2.1}$ (R1) thin films in ASTB at various current densities (130 µAh cm^{-2} ~ 2C rate), and **(D)** the respective evolution of both the volumetric capacity and the Coulombic efficiency. Reprinted with permission from Dubois et al. (2017). © 2017 ACS.

of active materials decreases slowly because of polarization. The battery also showed good rate capability with 74% capacity under 10°C rate. EIS measurements of the ASTB revealed a constant impedance for 4000 cycles which is not as severe as for that for liquid electrolyte.

Metal Oxides

Research into PVD of metal oxide thin films has been also progressing throughout the last two decades (Burdis 1997; Branci et al., 2000; Panagopoulou et al., 2017; Varghese et al., 2019). Early discovery of Lipon led researchers to fabricate thin-film batteries with V_2O_5 instead of conventional lithium transition metal oxide materials. Bates et al. fabricated V_2O_5 with Lipon electrolyte and Li metal and observed a reversible capacity of ~105 mC (i.e., 29.2 µAh) with an active area of 1 cm^2 and a cathode thickness of 1 µm (Bates et al., 1993). By tweaking the process parameters, later they were able to obtain a specific capacity of ~117.6 µAh cm^{-2} $µm^{-1}$ for a sample of size 1.21 cm^2 and a thickness of 0.13 µm (Bates et al., 1995a). The cathode films were observed to be amorphous in structure, and the resulting battery exhibited large polarization which arises from the slow diffusion of Li^+ in the cathode. Jeon et al. (2001) also fabricated V_2O_5 cathode from a vanadium target in an Ar/O_2 mixed environment. Batteries fabricated without exposure to ambient pressure and with exposure were compared. A V_2O_5/LiPON/Li-type battery was fabricated and showed better performance for *in situ* deposition of electrolyte (the cathode and electrolyte were deposited sequentially without venting the chamber) than for an *ex situ* situation. Although SEM images did not show evident surface features for the *ex situ* sample, EIS measurements claimed otherwise. Electrolyte resistance increased by ~4.5 times, while interfacial resistance increased by ~15 times for the *ex situ* sample and subsequently the charge transfer resistance was 10 times higher for the *ex situ* sample than for the *in situ* sample. Nevertheless, cyclic behavior was similar for both samples, although the *in situ* sample had a higher reversible capacity (~4.8 µAh and 3.5 µAh for *in situ* and *ex situ* batteries, respectively). Cystalline V_2O_5 was also investigated as cathode in ASTBs (Navone et al., 2009). Oxygen flow rate during sputtering determines the porous or dense crystalline structure of V_2O_5 films. XRD patterns indicated that thicker samples prefer a crystalline orientation of (110) and thinner ones prefer (h00). This behavior is similar to the results obtained by other groups (Bates et al., 2000; Tan et al., 2014). At a current density of

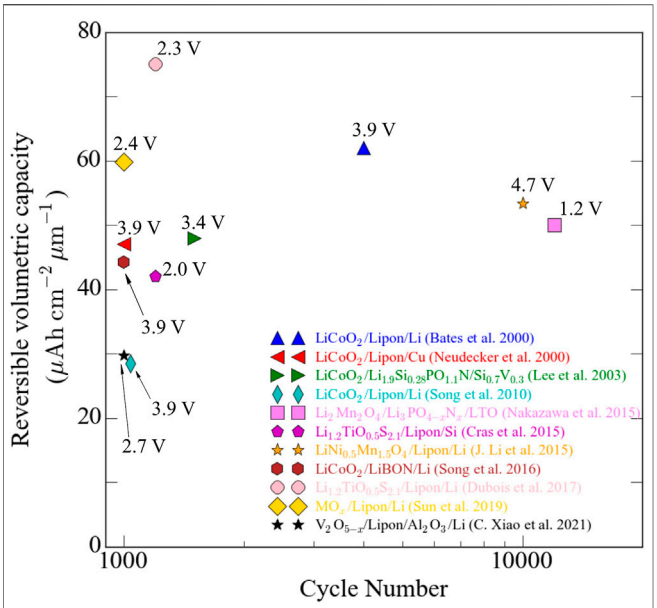

FIGURE 6 | Reversible volumetric capacity of selected ASTBs with approximate nominal voltages.

100 μAh cm^{-2}, a specific capacity of 25 μAh cm^{-2} μm^{-1} was obtained without any capacity fading over 100 cycles. In another study, oxygen-deficient V_2O_{5-x} showed good capacity (32.74 μAh cm^{-2} μm^{-1}) and a remarkable rate capability (up to 100°C) (Xiao et al., 2021). This was attributed to the 1-nm Al_2O_3 layer that was deposited between the electrolyte and Li. Although the voltage profile is linearly decreasing, the capacity could be maintained for 1000 cycles (**Figures 5A,B**).

Doping of oxides was also considered by several groups. Huang et al. produced $Li_xAg_{0.5}V_2O_5$ using the PLD technique and using various concentrations of Li_x (1,2,3,4) (Huang et al., 2003). With liquid electrolyte, $Li_2Ag_{0.5}V_2O_5$ had the highest capacity of 110 μAh cm^{-2} μm^{-1} with 10 μAh cm^{-2} current. XRD patterns revealed that the $Li_{0:33}V_2O_5$ diffraction peaks disappear after lithium insertion, which might be the result of the transformation of the polycrystalline structure into an amorphous phase. The ASTB with the above-mentioned cathode was cycled for 40 cycles, and the specific capacity faded from ~85 μAh cm^{-2} μm^{-1} to ~40 μAh cm^{-2} μm^{-1} at a current density of 7 μAh cm^{-2}. Still, this capacity is higher than that for the $Ag_{0:5}V_2O_5$ film cathode that was developed by the same group (Huang et al., 2004). Lee et al. also observed that Ag doping increases V_2O_5 performance (Lee et al., 2004). In particular, the $Ag_{0:8}V_2O_5$ cathode showed 78 μAh cm^{-2} μm^{-1} capacity, which it maintains for more than 200 cycles.

Another oxide cathode-based ASTB with MoO_3 cathode was developed by Ohtsuka and Yamaki (1989). The cathode film was reduced MoO_{3-x} due to sputtering, and (010) plane XRD peaks of Mo_9O_{26} ($MoO_{2.89}$) were found, confirming this. The cell exhibited a capacity of 60 μAh cm^{-2} μm^{-1} for 240 cycles. To increase the cell capacity per unit area, the group fabricated an ASTB with a thickness of 4.66 μm. With improved ionic conductivity of Li_2O–V_2O_5–SiO_2 thin-film electrolyte (1×10^{-6} S cm^{-1}), a cycling discharge capacity of 290 μAh cm^{-2} per unit area at 10 μAh cm^{-2} current was obtained. However, cathode utilization is estimated to be only 81.7% compared to that in a thinner sample of 1 μm. The discharge capacity decreased when the current densities increased as well. MoO_3/Lipon/Li ASTBs on glass and on flexible polyimide substrates were also fabricated (Glenneberg et al., 2016). The ASTB on the polyimide substrate has a slightly better discharge capacity than that on the glass substrate at low currents, but it is pronounced at higher current densities of 10°C (202.5 μAh cm^{-2}). The ASTB on the polyimide substrate shows a discharge capacity of 71.7 μAh cm^{-2} μm^{-1}, while that on the glass substrate has a value of 63.8 μAh cm^{-2} μm^{-1}. With a flexible substrate, the cells have less mechanical stress, and the Lipon therefore has better ionic conductivity. In addition, this results in lower electrolyte resistance, which is accompanied by higher lithium ion mobility and thus leads to higher capacity values. In addition, the impedance of the Lipon on the glass substrate and that on the polyimide are distinct. Unlike the glass substrate, battery layers on the polyimide substrate are mounted on the surface, there is no tension, and thus no reduced impedance can be measured. These results are also consistent with the results obtained for ASTBs on flexible substrates (Song et al., 2010; Koo et al., 2012; Song et al., 2016). All in all, MoO_3 material, although it has a small voltage window, shows a good cycle stability of at least 550 full cycles, with only slight capacity fading when fabricated on a flexible substrate. Sun et al. made self-standing oxygen-deficient α-MoO_{3-x} nanoflake arrays (Sun et al., 2019). Mo target was sputtered in an Ar/O_2 environment and 2D/3D structures were obtained for low/high deposition and at post-annealing temperatures. XRD and Raman spectroscopy confirm the crystallinity of both the cathode structures, but the 3D structured one has more preferred orientation on the (060) plane. TEM and SAED patterns also confirmed preferred orientation of 0k0 for nanoflakes. After sputtering, 2D and 3D α-MoO_{3-x} samples were oxygen deficient since XPS results showed Mo^{5+} ions. After depositing Lipon electrolyte layer and Li anode, a cross-sectional view of interfaces revealed a more smooth transition between Lipon and MoO_3 for the 3D sample. The cyclic performances were also compared. The 3D sample had a capacity retention of 92.7% [145 mAh g^{-1} (64.5 μAh cm^{-2} μm^{-1}) to ~140 mAh g^{-1} (59.8 μAh cm^{-2} μm^{-1})] after 1000 cycles, whereas the 2D sample had only 76% (90 mAh g^{-1} to ~70 mAh g^{-1}). In addition, 3D MoO_3 was demonstrated to be better off with solid electrolyte than with liquid electrolyte at high currents because it achieves improved accommodation capability for volume variation with enhanced structural and mechanical stability.

Liu et al. (2007) deposited Au/TiO_2/Lipon/Li sequentially without breaking vacuum and compared it with *ex situ* process, that is, TiO_2 was exposed to air. The *in situ* sample behaved very stable in than the *ex situ* sample. Although the thickness is very small (70 nm) and the *ex situ* sample decreases pretty well after 50 cycles. EIS measurements were performed at the beginning and at 50 cycles. By fitting, they found the interfacial resistance and charge transfer resistance to be 35 times higher than those in the *in situ* sample.

Sulfides, Phosphates, and Tungstates

Many research groups have used PVD to make sulfide/phosphate (including $LiFePO_4$)/tungstate electrodes for all solid-state thin-film batteries (Yufit et al., 2003; Mazor et al., 2009; Sugiawati et al., 2019; Ioanniti et al., 2020). Not many have actually demonstrated such ASTBs. Here, we report the groups that actually made ASTBs and not sufficed with one part of the battery.

Sulfides

Back in 1993, Bates et al. developed a TiS_2 cathode-based ASTB with a specific capacity of 75 μAh cm^{-2} $μm^{-1}$ (Bates J. B. et al., 1993). After being cycled for 4000 cycles, the SEM cross section exhibited a fracture between the layers of the battery. Also, Eveready Battery Company developed a TiS_2/6LiI-4Li_3PO_4-P_2S_5/Li battery with open circuit voltage (OCV) between 2.4 and 2.5 V and an energy density of 140 Wh L^{-1} (Jones, Akridge, and Middaugh 1999). This battery had reached 10,000 cycles at 100 μAh cm^{-2} and was still running at about 90% cathode utilization to a 1.4 V cutoff.

Later, the group at Centre National de la Recherche Scientifique (CNRS) developed a TiOS cathode for ASTBs (Fleutot et al., 2011). The integration of oxygen leads to the existence of two forms of sulfur species: S^{2-} as in TiS_2, and S_2^{2-} disulfide pairs as in TiS_3. At the beginning of lithium insertion (i.e., at higher voltage), these disulfide pairs found in TiO_yS_z can be minimized and help increase a positive electrode potential as compared to pure TiS_2. The chemical lithium diffusion coefficient was calculated from GITT experiments at 20°C, and it ranged mainly from 5×10^{-11} to 3×10^{-10} cm^2 s^{-1} between the compositions of $TiO_{0.6}S_{1.6}$ and $Li_{1.2}TiO_{0.6}S_{1.6}$. The ASTB was encapsulated with a polymer/metal multilayer to protect the active stack from moisture and oxygen and had a specific capacity of 90 μAh cm^{-2} $μm^{-1}$ when cycled at 100 μAh cm^{-2} $μm^{-1}$ between 1 and 3 V vs. Li^+/Li. However, there was a stable capacity fading, and this was correlated to the increase in cell impedance. The key cause of the capacity decline is consistent with the modification of the Li electrode morphology when charging, which resulted in a steady drop of the LiPON/Li contact area and a rise in internal resistance during the subsequent discharging. This was also seen in a previous study led by Neudecker et al. (2000). Inspired by the results, the group fabricated ASTBs with $Li_{1.2}TiO_{0.5}S_{2.1}$ (LiTiOS) and Si anode at different thicknesses (Cras et al., 2015). When Si is in excess capacity (180 nm thick) for a 1.1-μm positive electrode, irreversible processes occur at the LiPON/Si interface where "SiO_xN_y" species are formed during cycling. The same features were seen for Si/LiPON/Li half-cells. If the anode is less in capacity (80 nm thick), Si is not enough for alloying, so Li is plated between the LiPON/Si interface, which is also confirmed by differential capacity measurements. For capacity-balanced cells (120-nm–thick Si), more than 1200 cycles were achieved with LiTiOS/LiPON/(Si 120 nm) cells, leading to a mean capacity fading of about −0.015% per cycle. Li plating occurred for balanced cells as well if they were not discharged below 1.45 V due to the above reasons. This could be recovered by discharging to lower potentials. Furthermore, the Coulombic efficiency revealed that the Li inserted in a Si electrode was above the amount of Li collected during the subsequent discharge of the cell. This means that Li accumulates gradually in the negative electrode as a result of modifications in the Li_xSi electrode's voltage curve. Overall, a solder reflow tolerant ASTB was fabricated using PVD techniques. More studies of LiTOS fabricated by sputtering targets of $LiTiS_2$ in Ar were done by the group (Dubois et al., 2017). They chose several routes of target preparation, and the one that involved preparation of a $LiTiS_2$ powder by chemical lithiation of TiS_2 using n-butyl lithium (route R1) exhibited better thin films when it was used as a target. Ti^{4+} species were evidenced in XPS measurements only in the films that were prepared by sputtering of the target prepared by R1. These observations are completely compatible with the LiTiOS charge balance and mean that all the Ti^{3+} that was first present in $LiTiS_2$ is oxidized during the sputtering. S activity redox happens in the beginning of discharge and then Ti activity further increases the capacity (**Figures 5C,D**). In addition, when the state of charge is at 90–100%, contributions that may have been correlated with the creation of an interphase at Li_xTiOS/LiPON are seen. Diffusion coefficients measured in $Li_xTiO_{0.5}S_{2.1}$ materials are comparable or significantly higher than those for $LiCoO_2$ and $LiMn_2O_4$ materials.

The same group fabricated an ASTB based on sputtered pyrite electrodes (FeS_2), a Lipon electrolyte, and a Li anode (Pelé et al., 2015). The successive reduction of S_2^{2-} and Fe^{2+} species resulted in a five times higher volumetric discharge capacity than that of $LiCoO_2$. The first and subsequent 800 charge/discharge cycles were obtained with excellent reversibility (no irreversible capacity during first cycles <2%) and capacity retention. Discharging at higher potentials (3.5–1.5 V) was detrimental to the cathode, but recovery happened when returned to 3.5–0.5 V, and the initial capacity was easily recovered after few full oxidation cycles.

Phosphates

West et al. made a cathode of $LiCoPO_4$ (West et al., 2003). Cathodes, sputtered from the target prepared by solid-state reaction, showed a high nominal voltage of 4.8 V, with a lower plateau at 2.5 V corresponding to a much higher conductivity phase. Annealing at 700°C is required to obtain crystalline structures and grains of crystallites as confirmed by XRD and SEM results. Cathode layer resistance dipped at 2.5 V OCV and increased with increasing cell voltage until ~3.3 V. The ASTB had an initial specific discharge capacity of 11 μAh cm^{-2} $μm^{-1}$ at C/15 and it decreased steadily over the next 100 cycles. Amorphous iron phosphate $FePO_4$ and iron phosphorous oxynitride FePON thin-film cathodes were fabricated by the group at Fudan University (Li et al., 2006b). The $FePO_4$ target was sputtered in an Ar/O_2 mixture and in pure nitrogen to fabricate the respective cathodes. $FePO_4$ became more crystalline as the annealing temperature was increased to 600°C, yet it did not show better specific capacity. Only the 200°C annealed one showed a slightly better specific capacity than the as-deposited one (20 μAh cm^{-2} $μm^{-1}$ compared with 15 μAh cm^{-2} $μm^{-1}$). Cycling performance and CV of the ASTB with as-deposited and 200°C annealed cathodes exhibited similar characteristics, even though the as-deposited cathode had a lower diffusion coefficient than the 200°C annealed cathode. N incorporation into the O site can be observed from XPS studies of FePON cathode films. FePON thin films were 3.5 times more ionically conductive than $FePO_4$ thin films and can be charged to $Li_{1.1}$ because of N introducing more defects in the structure. The ASTB made out of FePON cathode was 63 μAh cm^{-2} $μm^{-1}$ and faded by 28% within 90 cycles.

Tungstate

Tungstate ASTBs were exclusively studied by the group at Fudan University. Nano-sized $CuWO_4$ thin films were tested with liquid and solid Lipon electrolytes (Li and Fu 2008b). ASTBs with $CuWO_4$/Lipon/Li layers showed a high specific capacity of 145 μAh cm^{-2} μm^{-1} in the first discharge at a current density of 14 μAh cm^{-2}, and overcame the unfavorable electrochemical degradation observed in the liquid electrolyte system. This high capacity is due to the extrusion and injection of Cu^{2+}/Cu^0, as well as the reversible reactivity of $(WO_4)^{2-}$ framework. However, the capacity quickly decreased to ~63 μAh cm^{-2} μm^{-1} at the 10th cycle, and the overall reversible capacity was 30 μAh cm^{-2} μm^{-1} after 100 cycles. Also, the group made $LiFe(WO_4)_2$ thin films that were sputtered from a target consisting of Li_2CO_3, Fe_2O_3, and WO_3 powders mixed at a molar ratio of 1:1:4 (Li and Fu 2008a). Amorphous thin films were crystallized upon cycling as proved by XRD and TEM patterns. Since there are two redox centers (Fe^{3+} and W^{6+}), there are two separate plateaus at 3 and 1.5 V. The initial discharge capacity is as large as 104 μAh cm^{-2} μm^{-1} and 56 μAh cm^{-2} μm^{-1} retained after 150 cycles, which is comparable to $LiCoO_2$ and $LiMn_2O_4$. Yet, there is an irreversible charge capacity of 29% which is due to kinetic constraints of the discharge phase, possible side reactions, and electrolyte oxidation during charging. Bi_2WO_6 thin-film cathodes were made using RF sputtering of the target that was produced by the solid-state reaction of Bi_2O_3 and WO_3 powders with a molar ratio of 1:1 (Li et al., 2009). The electrochemical properties of annealed Bi_2WO_6, annealed Bi_2O_3, and as-deposited WO_3 were compared with that of a liquid electrolyte. A multiple-center reactive mechanism associated with both Bi^{3+}/Bi^0 and W^{6+}/W^{x+} ($x < 6$) was observed by *ex situ* X-ray and TEM studies. The first discharge plateau of the Bi_2WO_6 thin film is lower than that of subsequent cycles but shows a much higher specific capacity. This is explained by the evolution of the Bi_2WO_6 reaction mechanism and structural modification of the original Aurivillius structure. The ASTB was cycled between 1.5 and 4 V and showed a capacity of 15 μAh cm^{-2}. However, the battery failed when discharge was lowered to 1 V, and this is attributed to the breakage of the electrolyte–electrode interface or Lipon short circuiting.

INTERFACES BETWEEN CATHODES AND SOLID ELECTROLYTES

Despite the optimistic future of solid-state batteries, the key obstacle to the successful production of solid-state batteries is the minimization of interface impedances between solid-state electrolytes and electrodes, particularly for cathode/SSE interfaces (Ding et al., 2020). There are several ways a cathode–electrolyte interface can degrade in ASTBs: 1) formation of a space charge layer, 2) reaction of the electrolyte with the cathode material, and 3) a decrease in physical contact between the layers upon cycling. To mitigate these, interface modifications on either electrodes or SSEs are necessary for successful operation of ASTBs. To stabilize the surface of cathode–electrolyte interfaces, surface coating and modification using ALD have been identified as a viable solution to reduce electrolyte decomposition and associated impedance increases (Meng, Yang, and Sun 2012; Jung et al., 2013; Wise et al., 2015). Ultrathin coating films using ALD are very uniform and highly precise on complex and large substrates (Liu et al., 2018). Although PVD cannot offer a uniform coating on highly textured substrates, several techniques do provide improvements (Xiao et al., 2021). Thermal annealing has been employed by groups as one of the solutions for the above. For example, by heating the Lipon electrolyte in contact with the $LiCoO_2$ cathode at 250°C for 10 min in air, the resistance of the bulk electrolyte and the charge-transfer resistance at the Lipon–$LiCoO_2$ interface were reduced by about a factor of 2 (Neudecker et al., 2000). Rapid thermal annealing of the cathode before electrolyte deposition has also proven as a solution because it can remove the surface oxide layer formed on the cathode and improve the cathode–electrolyte interface (Kim et al., 2004; Song et al., 2010; Liu et al., 2017). One group prepared electrode and electrolyte in the same vacuum chamber to prevent the formation of a possible resistive layer on the surface of the $LiCoO_2$ film, and from the impedance data, the interface resistance contributed only a little to the total resistance of the ASTB (Matsuda et al., 2018).

In addition, to improve the cathode–electrolyte interface, nanostructuring of the cathode layer was observed to improve interfacial stability. For instance, the $LiCoO_2$ nanorods of approximately ~100 nm width that are normal to the substrate show an impressive rate capability and can achieve 90% capacity in 5.9 min (~10°C) (Song et al., 2016). Also, small grains (~10 nm) of $LiMn_2O_4$ were formed after charge–discharge cycling of the amorphous $Li_2Mn_2O_4$ matrix (Nakazawa et al., 2015). These are spinel grains with well-formed tetrahedral 8a sites. This ASTB showed quite stable cycle performance over more than 10,000 cycles. Moreover, thin-film cathodes of α-MoO_{3-x} that have vertically aligned nanoflakes of about 40–60 nm thickness show superior electrochemical performance, maximizing the cathode–electrolyte interface while retaining the short Li^+ diffusion length (Sun et al., 2019). The 3D nanowall architecture of $LiMn_2O_4$ and Li_xMnO_2 has also shown greater performance than the 2D counterparts (Xia et al., 2018; Xia et al., 2020). A significant increase in the cathode–electrolyte interface area and improved accommodation capability for volume change provide fast ion transport and enhanced structural and mechanical stability. Therefore, nanostructuring of the cathode layer improves interfacial stability. Protecting ASTBs with Li anode against ambient conditions is also important for high cycle stability. It has been shown by SEM that during electrochemical cycling, the overlayer is essential for ASTBs; otherwise, the battery loses most of its capacity within a few cycles since the plated Li rapidly develops a detrimental morphology (Neudecker et al., 2000). Furthermore, as confirmed by XPS tests, ASTBs with Al anode demonstrated rapid capacity fading due to the development of an insulating Al–Li–O ternary alloy on the top surface of a negative electrode (Gong et al., 2015). Multilayer encapsulation (polymer/metal) was also made for Si-based ASTBs, and this reinforced by a glass slide provided long duration cycling (Phan et al., 2012).

In addition, it was claimed that during deposition of Lipon, N_2 plasma abuses the top surface of $LiCoO_2$ and induces defects, which creates a space charge layer (Xiao et al., 2018). However, another group performed an *in situ* electron energy loss

spectroscopy observation of $LiCoO_2$/Lipon/Si fabricated by sputtering, and they showed that it is unlikely that the disordered layer was formed as a result of the sputter deposition process of Lipon on $LiCoO_2$. During *in situ* charging, the interface layer between the cathode and the electrolyte led to the formation of a strongly oxidized Co ion species alongside species of lithium oxide and lithium peroxide. These results indicate that the interfacial impedance process at $LiCoO_2$/Lipon is triggered by chemical changes rather than by the space charge effect (Wang et al., 2016).

CONCLUSION AND OUTLOOK

Vacuum-based technology for fabrication of all solid-state thin-film batteries has proven to be excellent to control the film structure and morphology that have been used in the design of cathode materials. In this review, we documented the usage of PVD techniques for the synthesis of cathode materials for ASTBs coupled with solid-state electrolytes and anodes. We based our report on planar batteries whose specific capacity is bounded by area as opposed to 3D microbatteries. However, 3D ASTBs have proved to be very difficult to technologically accomplish, and the promise of a high energy and power density battery is yet to be fulfilled. Nevertheless, there are commercially available 2D ASTBs with high areal capacity (>250 μAh cm^{-2}), and several groups have shown very promising works involving planar ASTBs (**Figure 6**). Fabrication of cathodes using PVD methods can be summarized as follows:

1. RF sputtering technique can provide thin-film cathodes that can deliver satisfactory electrochemical performance without binders or conductive supplements.
2. Post-annealing of cathodes could be replaced by RTA techniques which are operated at lower temperatures.
3. Bias sputtering or heating substrates during deposition could be a viable method for fabrication of cathodes with suitable properties.
4. Lipon SSE is the main electrolyte for studying cathodes with various chemistries.

Electrochemical properties of ASTBs based on cathode materials of lithium transition metal oxides, metal oxides, lithium phosphates, sulfide, and tungstate materials were reported. **Figure 5** shows the reversible volumetric capacity, the approximate nominal voltage, and the cathode chemistry of ASTBs that were cycled more than 1000 times.

In addition, routes that were used by research groups to mitigate electrode–electrolyte interfacial resistance are also discussed. The primary limitation of ASTBs is the cathode–electrolyte interface whose properties are degraded due to the formation of a space charge layer, reaction of electrolyte with cathode material, and loss of physical contact between the layers upon cycling. To mitigate these, the following perspective solutions were proposed by research groups:

1. Thermal annealing of the substrate after cathode and electrolyte deposition, which could improve the physical contact between the layers and prevent delamination.
2. Nanostructuring of cathodes for battery cathode–electrolyte interfaces, which could be achieved by adjusting the deposition parameters.
3. Deposition of a thin buffer layer between cathode–electrolyte interfaces, which proved to improve the electrochemical properties.

Furthermore, electrodes of ASTBs require an appropriate protective layer that needs to be electrochemically stable against lithium and nonpenetrable for air. To date, ASTBs including $LiCoO_2$ thin-film cathode and Lipon electrolyte are mature, and new emerging cathodes need to be tested and studied with promising electrolyte materials.

Noteworthy is the fact that PVD techniques still face some challenges, which include the following:

1. Low deposition rates of refractory materials
2. Obtaining lithium-deficient electrolyte or electrode during PVD depositions
3. Detrimental effect of plasma on the cathode electrode surface during sputter deposition of electrolyte

Future directions of PVD should be concentrated on the above challenges, thus decreasing the detrimental effect on electrode–electrolyte interfaces. Overall, thin-film cathodes represent a critical basis for advanced lithium ion batteries, but developing a promising thin-film cathode using more efficient methods requires significant efforts.

AUTHOR CONTRIBUTIONS

BU drafted the manuscript. AM and YZ helped with critical revision of the manuscript. ZB revised and approved the final version to be published.

FUNDING

This work was funded by the Faculty Development Competitive Research Grant Program (FDCRGP) No. 110119FD4504 of Nazarbayev University titled "Development of 3D solid state thin film materials for durable and safe Li-ion microbatteries" and a project AP08052231 "Development of solid electrolytes with high ionic conductivity for the next generation lithium-ion batteries" from the Ministry of Education and Science of the Republic of Kazakhstan.

SUPPLEMENTARY MATERIAL

The Supplementary Material for this article can be found online at: https://www.frontiersin.org/articles/10.3389/fenrg.2021.625123/full#supplementary-material

REFERENCES

Baba, M., Kumagai, N., Fujita, N., Ohta, K., Nishidate, K., Komaba, S., et al. (2001). Fabrication and Electrochemical Characteristics of All-Solid-State Lithium-Ion Rechargeable Batteries Composed of LiMn2O4 Positive and V2O5 Negative Electrodes. *J. Power Sourc.* 97-98 (98), 798–800. doi:10.1016/s0378-7753(01)00733-9

Baskaran, R., Kuwata, N., Kamishima, O., Kawamura, J., and Selvasekarapandian, S. (2009). Structural and Electrochemical Studies on Thin Film LiNi0.8Co0.2O2 by PLD for Micro Battery. *Solid State Ionics* 180 (6–8), 636–643. doi:10.1016/j.ssi.2008.11.012

Bates, J. B., Dudney, N. J., Gruzalski, G. R., Zuhr, R. A., Choudhury, A., Luck, C. F., et al. (1992). SOLID STATE IONICS Electrical Properties of Amorphous Lithium Electrolyte Thin Films. *Sohd State Iomcs* 56, 53–56. doi:10.1016/0167-2738(92)90442-R

Bates, J. B., Dudney, N. J., Gruzalski, G. R., Zuhr, R. A., Choudhury, A., Luck, C. F., et al. (1993). Fabrication and Characterization of Amorphous Lithium Electrolyte Thin Films and Rechargeable Thin-Film Batteries. *J. Power Sourc.* 43 (1–3), 103–110. doi:10.1016/0378-7753(93)80106-y

Bates, J. B., Dudney, N. J., Lubben, D. C., Gruzalski, G. R., Kwak, B. S., Yu, X., et al. (1995). Thin-Film Rechargeable Lithium Batteries. *J. Power Sourc.* 54 (1), 58–62. doi:10.1016/0378-7753(94)02040-a

Bates, J. B., Gruzalski, G. R., Dudney, N. J., Luck, C. F., and Yu, X. (1993a). THIN-FILM RECHARGEABLE LITHIUM BATTERIES, Proc. 8th Electronic Materials and Processing Congress, August–2 September, 30 San Jose, CA, USA

Bates, J. B., Lubben, D., Dudney, N. J., and Hart, F. X. (1995a). 5 Volt Plateau in LiMn2 O 4 Thin Films. *J. Electrochem. Soc.* 142 (9), L149–L151. doi:10.1149/1.2048729

Bates, J. B., Dudney, N. J., Neudecker, B. J., Hart, F. X., Jun, H. P., and Hackney, S. A. (2000). Preferred Orientation of Polycrystalline LiCoO[Sub 2] Films. *J. Electrochem. Soc.* 147 (1), 59. doi:10.1149/1.1393157

Bates, J., Dudney, N. J., Neudecker, B., Ueda, A., and Evans, C. D. (2000a). Thin-Film Lithium and Lithium-Ion Batteries. *Solid State Ionics* 135 (1–4), 33–45. doi:10.1016/s0167-2738(00)00327-1

Branci, C., Benjelloun, N., Sarradin, J., and Ribes, M. (2000). Vitreous Tin Oxide-Based Thin Film Electrodes for Li-Ion Micro-batteries. *Solid State Ionics* 135 (1–4), 169–174. doi:10.1016/s0167-2738(00)00297-6

Bünting, A., Uhlenbruck, S., Sebold, D., Buchkremer, H. P., and Vaßen, R. (2015). Three-Dimensional, Fibrous Lithium Iron Phosphate Structures Deposited by Magnetron Sputtering. *ACS Appl. Mater. Inter.* 7 (40), 22594–22600. doi:10.1021/acsami.5b07090

Burdis, M. S. (1997). Properties of Sputtered Thin Films of Vanadium-Titanium Oxide for Use in Electrochromic Windows. *Thin Solid Films* 311 (1–2), 286–298. doi:10.1016/s0040-6090(97)00724-4

Chen, P. C., Shen, G., Sukcharoenchoke, S., and Zhou, C. (2009). Flexible and Transparent Supercapacitor Based on In2 O 3 Nanowire/Carbon Nanotube Heterogeneous Films. *Appl. Phys. Lett.* 94 (4), 2007–2010. doi:10.1063/1.3069277

Cras, F. L., Pecquenard, B., Dubois, V., Phan, V., and Guy-Bouyssou, D. (2015). All-Solid-State Lithium-Ion Microbatteries Using Silicon Nanofilm Anodes: High Performance and Memory Effect. *Adv. Energ. Mater.* 5 (19), 1–10. doi:10.1002/aenm.201501061

Dasgupta, N. P., Meng, X., Elam, J. W., and Martinson, A. B. F. (2015). Atomic Layer Deposition of Metal Sulfide Materials. *Acc. Chem. Res.* 48 (2), 341–348. doi:10.1021/ar500360d

Ding, J. J., Sun, Q., and Zheng, W. (2010). Layered Li(Ni1/4Mn1/2Co13)O2 as Cathode Material for All-Solid-State Thin-Film Rechargeable Lithium-Ion Batteries. *Electrochem. Solid-State Lett.* 13 (8), 108–111. doi:10.1149/1.3432254Fu

Ding, Z., Li, J., Li, J., and An, C. (2020). "Review—Interfaces: Key Issue to Be Solved for All Solid-State Lithium Battery Technologies. *J. Electrochem. Soc.* 167 (7), 070541. doi:10.1149/1945-7111/ab7f84

Dubois, V., Pecquenard, B., Soule, S., Martinez, H., and Le Cras, F. (2017). Dual Cation-And Anion-Based Redox Process in Lithium Titanium Oxysulfide Thin Film Cathodes for All-Solid-State Lithium-Ion Batteries. *ACS Appl. Mater. Inter.* 9 (3), 2375–2384. doi:10.1021/acsami.6b11987

Dudney, N. J. (2008). Thin Film Micro-batteries. *Electrochem. Soc. Interf.* 17 (3), 44–48. doi:10.1149/2.f04083if

Fenech, M., and Sharma, N. (2020). Pulsed Laser Deposition-based Thin Film Microbatteries. *Chem. Asian J.* 15 (12), 1829–1847. doi:10.1002/asia.202000384

Feng, J., Yan, B., Lai, M. O., and Li, L. (2014). Design and Fabrication of an All-Solid-State Thin-Film Li-Ion Microbattery with Amorphous TiO2as the Anode. *Energ. Techn.* 2 (4), 397–400. doi:10.1002/ente.201300173

Fleutot, B., Pecquenard, B., Cras, F. L., Delis, B., Martinez, H., Dupont, L., and Guy-Bouyssou, D. (2011). Characterization of All-Solid-State Li/LiPONB/TiOS Microbatteries Produced at the Pilot Scale. *J. Power Sourc.* 196 (23), 10289–10296. doi:10.1016/j.jpowsour.2011.07.018

Gandla, D., and Tan, D. Q. (2019). Progress Report on Atomic Layer Deposition toward Hybrid Nanocomposite Electrodes for Next Generation Supercapacitors. *Adv. Mater. Inter.* 6 (16), 1–21. doi:10.1002/admi.201900678

Glenneberg, J., Andre, F., Bardenhagen, I., Langer, F., Schwenzel, J., and Kun, R. (2016). A Concept for Direct Deposition of Thin Film Batteries on Flexible Polymer Substrate. *J. Power Sourc.* 324, 722–728. doi:10.1016/j.jpowsour.2016.06.007

Gong, C., Ruzmetov, D., Pearse, A., Ma, D., Munday, J. N., Rubloff, G., et al. (2015). Surface/Interface Effects on High-Performance Thin-Film All-Solid-State Li-Ion Batteries. *ACS Appl. Mater. Inter.* 7 (47), 26007–26011. doi:10.1021/acsami.5b07058

Han, B., Xu, D., Chi, S.-S., He, D., Zhang, Z., Du, L., et al. (2020). 500 Wh Kg-1 Class Li Metal Battery Enabled by a Self-Organized Core-Shell Composite Anode. *Adv. Mater.* 32, e2004793–11. doi:10.1002/adma.202004793

Huang, F., Fu, Z. W., Chu, Y. Q., Liu, W. Y., and Qin, Q. Z. (2004). Characterization of Composite 0.5Ag:V2O5 Thin-Film Electrodes for Lithium-Ion Rocking Chair and All-Solid-State Batteries. *Electrochem. Solid-State Lett.* 7 (7), 180–184. doi:10.1149/1.1736591

Huang, F., Zheng, W., and Qi, Z. (2003). A Novel Li2Ag0.5V2O5 Composite Film Cathode for All-Solid-State Lithium Batteries. *Electrochemistry Commun.* 5 (3), 262–266. doi:10.1016/s1388-2481(03)00036-5

Ioanniti, M. M., Hu, F., and Tenhaeff, W, E. (2020). Energy-Dense Li Metal Anodes Enabled by Thin Film Electrolytes. *J. Vacuum Sci. Techn. A* 38 (6), 060801. doi:10.1116/6.0000430

Jain, A., Ong, S. P., Hautier, G., Chen, W., Richards, W. D., Dacek, S., et al. (2013). Commentary: The Materials Project: A Materials Genome Approach to Accelerating Materials Innovation. *APL Mater.* 1 (1). doi:10.1063/1.4812323

Jang, Y.-I., Dudney, N. J., Blom, D. A., and Allard, L. F. (2003). Electrochemical and Electron Microscopic Characterization of Thin-Film LiCoO2 Cathodes under High-Voltage Cycling Conditions. *J. Power Sourc.* 119-121 (121), 295–299. doi:10.1016/s0378-7753(03)00160-5

Jeon, E. J., Shin, Y. W., Nam, S. C., Cho, W. L., and Yoon, Y. S. (2001). Characterization of All-Solid-State Thin-Film Batteries with V[Sub 2]O[Sub 5] Thin-Film Cathodes Using *Ex Situ* and *In Situ* Processes. *J. Electrochem. Soc.* 148 (4), A318. doi:10.1149/1.1354609

Jones, S. D., Akridge, J. R., and Middaugh, R. L. (1999). Development and Performance of a Rechargeable Thin Film Solid State Microbattery. *Mater. Res. Soc. Symp. - Proc.* 548, 695–700. doi:10.1557/PROC-548-695

Jung, Y. S., Lu, P., Cavanagh, A. S., Ban, C., Kim, G.-H., Lee, S.-H., George, S. M., Harris, S. J., and Dillon, A. C. (2013). Unexpected Improved Performance of ALD Coated LiCoO2/Graphite Li-Ion Batteries. *Adv. Energ. Mater.* 3 (2), 213–219. doi:10.1002/aenm.201200370

Kim, H.-K., Seong, T.-Y., Cho, W. i., and Yoon, Y. S. (2002). Rapid Thermal Annealing Effect on Surface of LiNi1−xCoxO2 Cathode Film for Thin-Film Microbattery. *J. Power Sourc.* 109 (1), 178–183. doi:10.1016/s0378-7753(02)00046-0

Kim, H, K., Seong, T.-Y., and Yoon, Y. S. (2002a). Fabrication of a Thin Film Battery Using a Rapid-Thermal-Annealed LiNiO2 Cathode. *Electrochem. Solid-State Lett.* 5 (11), 252–255. doi:10.1149/1.1510323

Kim, H, K., Seong, T.-Y., and Yoon, Y. S. (2004). Characteristics of Rapid-Thermal-Annealed LiNi1-XCo XO2 Cathode Films for All-Solid-State Rechargeable Thin Film Microbatteries. *Thin Solid Films* 447-448, 619–625. doi:10.1016/j.tsf.2003.07.024

Koo, M., Park, K.-I., Lee, S. H., Suh, M., Jeon, D. Y., Choi, J. W., Kang, K., and Lee, K. J. (2012). Bendable Inorganic Thin-Film Battery for Fully Flexible Electronic Systems. *Nano Lett.* 12 (9), 4810–4816. doi:10.1021/nl302254v

Kozen, A. C., Lin, C.-F., Pearse, A. J., Schroeder, M. A., Han, X., Hu, L., Lee, S.-B., Rubloff, G. W., and Noked, M. (2015). Xiaogang Han, Liangbing Hu, Sang Bok Lee, Gary W. Rubloff, and Malachi Noked.Next-Generation Lithium Metal Anode Engineering via Atomic Layer Deposition. *ACS Nano* 9 (6), 5884–5892. doi:10.1021/acsnano.5b02166

Kuwata, N., Kawamura, J., Toribami, K., Hattori, T., and Sata, N. (2004). Thin-Film Lithium-Ion Battery with Amorphous Solid Electrolyte Fabricated by Pulsed Laser Deposition. *Electrochemistry Commun.* 6 (4), 417–421. doi:10.1016/j.elecom.2004.02.010

Kuwata, N., Kumar, R., Toribami, K., Suzuki, T., Hattori, T., and Kawamura, J. (2006). Thin Film Lithium Ion Batteries Prepared Only by Pulsed Laser Deposition. *Solid State Ionics* 177 (26-32), 2827–2832. doi:10.1016/j.ssi.2006.07.023

Kyerematen, N. A., and Hahn., R. (2018). Attainable Energy Density of Microbatteries. *ACS Energ. Lett.* 3 (5), 1172–1175. doi:10.1021/acsenergylett.8b00500

Lacivita, V., Westover, A. S., Kercher, A., Phillip, N. D., Yang, G., Veith, G., Ceder, G., and Dudney, N. J. (2018). Resolving the Amorphous Structure of Lithium Phosphorus Oxynitride (Lipon). *J. Am. Chem. Soc.* 140 (35), 11029–11038. doi:10.1021/jacs.8b05192

Larfaillou, S., Guy-Bouyssou, D., Le Cras, F., and Franger, S. (2016). Comprehensive Characterization of All-Solid-State Thin Films Commercial Microbatteries by Electrochemical Impedance Spectroscopy. *J. Power Sourc.* 319, 139–146. doi:10.1016/j.jpowsour.2016.04.057

Lee, S.-J., Baik, H.-K., and Lee, S.-M. (2003). An All-Solid-State Thin Film Battery Using LISIPON Electrolyte and Si-V Negative Electrode Films. *Electrochemistry Commun.* 5 (1), 32–35. doi:10.1016/s1388-2481(02)00528-3

Lee, J. M., Hwang, H.-S., Cho, W.-I., Cho, B.-W., and Kim, K. Y. (2004). Effect of Silver Co-sputtering on Amorphous V2O5 Thin-Films for Microbatteries. *J. Power Sourc.* 136 (1), 122–131. doi:10.1016/j.jpowsour.2004.05.051

Li, C.-l., Liu, W.-y., and Fu, Z.-w. (2006). Physical and Electrochemical Characterization of LiCo0.8M0.2O2 (M=Ni,Zr) Cathode Films for All-Solid-State Rechargeable Thin-Film Lithium Batteries. *Chin. J. Chem. Phys.* 19 (6), 493–498. doi:10.1360/cjcp2006.19(6).493.6

Li, C.-L., Zhang, B., and Fu, Z.-W. (2006a). Physical and Electrochemical Characterization of Thin Films of Iron Phosphate and Nitrided Iron Phosphate for All-Solid-State Batteries. *J. Electrochem. Soc.* 153 (9), E160. doi:10.1149/1.2218110

Li, C.-L., Zhang, B., and Fu, Z.-W. (2006b). Physical and Electrochemical Characterization of Amorphous Lithium Lanthanum Titanate Solid Electrolyte Thin-Film Fabricated by E-Beam Evaporation. *Thin Solid Films* 515 (4), 1886–1892. doi:10.1016/j.tsf.2006.07.026

Liu, W.-Y., Fu, Z.-W., and Qin, Q.-Z. (2007). A Sequential Thin-Film Deposition Equipment for In-Situ Fabricating All-Solid-State Thin Film Lithium Batteries. *Thin Solid Films* 515 (7–8), 4045–4048. doi:10.1016/j.tsf.2006.10.111

Li, C.-L., and Fu, Z.-W. (2007). All-Solid-State Rechargeable Thin Film Lithium Batteries with LixMn2O4 and LixMn2O4-0.5ZrO2 Cathodes. *Electrochimica Acta* 52 (20), 6155–6164. doi:10.1016/j.electacta.2007.04.012

Li, C.-L., and Fu, Z.-W. (2008a). Electrochemical Characterization of Amorphous LiFe(WO4) 2 Thin Films as Positive Electrodes for Rechargeable Lithium Batteries. *Electrochimica Acta* 53 (22), 6434–6443. doi:10.1016/j.electacta.2008.04.063

Li, C.-L., and Fu, Z.-W. (2008b). Nano-Sized Copper Tungstate Thin Films as Positive Electrodes for Rechargeable Li Batteries. *Electrochimica Acta* 53 (12), 4293–4301. doi:10.1016/j.electacta.2008.01.014

Li, C.-L., Sun, K., Yu, L., and Fu, Z.-W. (2009). Electrochemical Reaction of Lithium with Orthorhombic Bismuth Tungstate Thin Films Fabricated by Radio-Frequency Sputtering. *Electrochimica Acta* 55 (1), 6–12. doi:10.1016/j.electacta.2009.04.037

Li, D., Ma, Z., Xu, J., Li, Y., and Xie, K. (2014). High Temperature Property of All-Solid-State Thin Film Lithium Battery Using LiPON Electrolyte. *Mater. Lett.* 134, 237–239. doi:10.1016/j.matlet.2014.07.092

Li, J., Cheng, M., Chi, M., Liang, C., and Dudney, N. J. (2015). Solid Electrolyte: The Key for High-Voltage Lithium Batteries. *Adv. Energ. Mater.* 5 (4). doi:10.1002/aenm.201570018

Lidor-Shalev, O., Yemini, R., Leifer, N., Nanda, R., Tibi, A., Perelshtein, I., Avraham, E. S., Mastai, Y., and Noked, M. (2019). Growth of Hybrid Inorganic/Organic Chiral Thin Films by Sequenced Vapor Deposition. *ACS Nano* 13 (9), 10397–10404. doi:10.1021/acsnano.9b04180

Liu, B., Fu, K., Gong, Y., Yang, C., Yao, Y., Wang, Y., Wang, C., Kuang, Y., Pastel, G., Xie, H., Wachsman, E. D., and Hu, L. (2017). Rapid Thermal Annealing of Cathode-Garnet Interface toward High-Temperature Solid State Batteries. *Nano Lett.* 17 (8), 4917–4923. doi:10.1021/acs.nanolett.7b01934

Liu, J., Zhu, H., Mohammad, H., and Shiraz, A. (2018). Toward 3D Solid-State Batteries via Atomic Layer Deposition Approach. *Front. Energ. Res.* 6, 1–5. doi:10.3389/fenrg.2018.00010

Liu, J., Bao, Z., Cui, Y., Dufek, E. J., Goodenough, J. B., Khalifah, P., Li, Q., Liaw, B. Y., Liu, P., Manthiram, A., Meng, Y. S., Subramanian, V. R., Toney, M. F., Viswanathan, V. V., Whittingham, M. S., Xiao, J., Xu, W., Yang, J., Yang, X.-Q., and Zhang, J.-G. (2019). Pathways for Practical High-Energy Long-Cycling Lithium Metal Batteries. *Nat. Energ.* 4 (3), 180–186. doi:10.1038/s41560-019-0338-x

Matsuda, Y., Kuwata, N., and Kawamura, J. (2018). Thin-film Lithium Batteries with 0.3-30 μm Thick LiCoO2 Films Fabricated by High-Rate Pulsed Laser Deposition. *Solid State Ionics* 320, 38–44. doi:10.1016/j.ssi.2018.02.024

Mazor, H., Golodnitsky, D., Burstein, L., and Peled, E. (2009). High Power Copper Sulfide Cathodes for Thin-Film Microbatteries. *Electrochem. Solid-State Lett.* 12 (12). doi:10.1149/1.3240921

Meng, X., Yang, X.-Q., and Sun, X. (2012). Emerging Applications of Atomic Layer Deposition for Lithium-Ion Battery Studies. *Adv. Mater.* 24 (27), 3589–3615. doi:10.1002/adma.201200397

Nakazawa, H., Sano, K., Abe, T., Baba, M., and Kumagai, N. (2007). Charge-Discharge Characteristics of All-Solid-State Thin-Filmed Lithium-Ion Batteries Using Amorphous Nb2O5 Negative Electrodes. *J. Power Sourc.* 174 (2), 838–842. doi:10.1016/j.jpowsour.2007.06.226

Nakazawa, H., Sano, K., and Baba, M. (2005). Fabrication by Using a Sputtering Method and Charge-Discharge Properties of Large-Sized and Thin-Filmed Lithium Ion Rechargeable Batteries. *J. Power Sourc.* 146 (1–2), 758–761. doi:10.1016/j.jpowsour.2005.03.155

Nakazawa, H., Sano, K., Baba, M., and Kumagai, N. (2015). Stability of Thin-Film Lithium-Ion Rechargeable Batteries Fabricated by Sputtering Method without Heating. *J. Electrochem. Soc.* 162 (3), A392–A397. doi:10.1149/2.0491503jes

Navone, C., Baddour-Hadjean, R., Pereira-Ramos, J. P., and Salot, R. (2009). Sputtered Crystalline V[Sub 2]O[Sub 5] Thin Films for All-Solid-State Lithium Microbatteries. *J. Electrochem. Soc.* 156 (9), A763. doi:10.1149/1.3170922

Navone, C., Tintignac, S., Pereira-Ramos, J. P., Baddour-Hadjean, R., and Salot, R. (2011). Electrochemical Behaviour of Sputtered C-V2o5 and LiCoO2 Thin Films for Solid State Lithium Microbatteries. *Solid State Ionics* 192 (1), 343–346. doi:10.1016/j.ssi.2010.04.023

Neudecker, B. J., Dudney, N. J., and Bates, J. B. (2000). "Lithium-Free" Thin-Film Battery with *In Situ* Plated Li Anode. *J. Electrochem. Soc.* 147 (2), 517. doi:10.1149/1.1393226

Ohtsuka, H., and Sakurai, Y. (2001). Characteristics of Li/MoO3â"x Thin Film Batteries. *Solid State Ionics* 144 (1–2), 59–64. doi:10.1016/s0167-2738(01)00889-x

Ohtsuka, H., and Yamaki, J.-I. (1989). Electrical Characteristics of Li2O_V2O5_SiO2 Thin Films. *Solid State Ionics* 35 (3–4), 201–206. doi:10.1016/0167-2738(89)90296-8

Oudenhoven, J. F. M., Baggetto, L., and Notten, P. H. L. (2011). All-Solid-State Lithium-Ion Microbatteries: A Review of Various Three-Dimensional Concepts. *Adv. Energ. Mater.* 1 (1), 10–33. doi:10.1002/aenm.201000002

Panagopoulou, M., Vernardou, D., Koudoumas, E., Katsarakis, N., Tsoukalas, D., Raptis, Y. S., and Raptis (2017). Tunable Properties of Mg-Doped V2O5 Thin Films for Energy Applications: Li-Ion Batteries and Electrochromics. *J. Phys. Chem. C* 121 (1), 70–79. doi:10.1021/acs.jpcc.6b09018

Park, H. Y., Lee, S. R., Lee, Y. J., Cho, B. W., and Cho, W. I. (2005). Bias Sputtering and Characterization of LiCoO2 Thin Film Cathodes for Thin Film Microbattery. *Mater. Chem. Phys.* 93 (1), 70–78. doi:10.1016/j.matchemphys.2005.02.024

Park, J. O., Kim, M., Kim, J. H., and Kyoung, H. (2019). Choi, Heung Chan Lee, Wonsung Choi, Sang Bok Ma, and Dongmin Im. 2019. "A 1000 Wh Kg−1 Li–Air Battery: Cell Design and Performance. *J. Power Sourc.* 419, 112–118. doi:10.1016/j.jpowsour.2019.02.057

Park, M. S., Wang, G. X., Liu, H. K., and Dou, S. X. (2006). Electrochemical Properties of Si Thin Film Prepared by Pulsed Laser Deposition for Lithium Ion Micro-batteries. *Electrochimica Acta* 51 (25), 5246–5249. doi:10.1016/j.electacta.2006.01.045

Park, Y.-S., Lee, S. H., Lee, B. I., and Joo, S. K. (1999). All-Solid-State Lithium Thin-Film Rechargeable Battery with Lithium Manganese Oxide. *Electrochem. Solid-state Lett.* 2 (2), 58–59. doi:10.1149/1.1390733

Pelé, V., Flamary, F., Bourgeois, L., Pecquenard, B., and Le Cras, F. (2015). Perfect Reversibility of the Lithium Insertion in FeS2: The Combined Effects of All-Solid-State and Thin Film Cell Configurations. *Electrochemistry Commun.* 51, 81–84. doi:10.1016/j.elecom.2014.12.009

Phan, V. P., Pecquenard, B., and Le Cras, F. (2012). High-Performance All-Solid-State Cells Fabricated with Silicon Electrodes. *Adv. Funct. Mater.* 22 (12), 2580–2584. doi:10.1002/adfm.201200104

Put, B., Vereecken, P. M., and Stesmans, A. (2018). On the Chemistry and Electrochemistry of LiPON Breakdown. *J. Mater. Chem. A.* 6 (11), 4848–4859. doi:10.1039/c7ta07928a

Qiao, Y., Deng, H., He, P., and Zhou, H. (2020). A 500 Wh/Kg Lithium-Metal Cell Based on Anionic Redox. *Joule* 4 (7), 1445–1458. doi:10.1016/j.joule.2020.05.012

Saccoccio, M., Yu, J., Lu, Z., Kwok, S. C. T., Wang, J., Yeung, K. K., Yuen, M. M. F., Ciucci, F., and Ciucci, F. (2017). Low Temperature Pulsed Laser Deposition of Garnet Li 6.4 La 3 Zr 1.4 Ta 0.6 O 12 Films as All Solid-State Lithium Battery Electrolytes. *J. Power Sourc.* 365, 43–52. doi:10.1016/j.jpowsour.2017.08.020

Schwenzel, J., Thangadurai, V., and Weppner, W. (2006). Developments of High-Voltage All-Solid-State Thin-Film Lithium Ion Batteries. *J. Power Sourc.* 154 (1), 232–238. doi:10.1016/j.jpowsour.2005.03.223

Singh, M., Kaiser, J., and Hahn, H. (2015). Thick Electrodes for High Energy Lithium Ion Batteries. *J. Electrochem. Soc.* 162 (7), A1196–A1201. doi:10.1149/2.0401507jes

Song, S.-W., Choi, H., Park, H. Y., Park, G. B., Lee, K. C., and Lee, H.-J. (2010). High Rate-Induced Structural Changes in Thin-Film Lithium Batteries on Flexible Substrate. *J. Power Sourc.* 195 (24), 8275–8279. doi:10.1016/j.jpowsour.2010.06.113

Song, S.-W., Lee, K.-C., and Park, H.-Y. (2016). High-Performance Flexible All-Solid-State Microbatteries Based on Solid Electrolyte of Lithium Boron Oxynitride. *J. Power Sourc.* 328, 311–317. doi:10.1016/j.jpowsour.2016.07.114

Sugiawati, V. A., Vacandio, F., Perrin-Pellegrino, C., Galeyeva, A., Kurbatov, A. P., and Djenizian, T. (2019). Sputtered Porous Li-Fe-P-O Film Cathodes Prepared by Radio Frequency Sputtering for Li-Ion Microbatteries. *Scientific Rep.* 9 (1), 11172. doi:10.1038/s41598-019-47464-2

Sun, S., Xia, Q., Liu, J., Xu, J., Zan, F., Yue, J., Savilov, S. V., Lunin, V. V., and Xia, H. (2019). Self-standing Oxygen-Deficient α-MoO3-x Nanoflake Arrays as 3D Cathode for Advanced All-Solid-State Thin Film Lithium Batteries. *J. Materiomics* 5 (2), 229–236. doi:10.1016/j.jmat.2019.01.001

Talin, A. A., Ruzmetov, D., Kolmakov, A., McKelvey, K., Ware, N., El Gabaly, F., Dunn, B., and White, H. S. (2016). Fabrication, Testing, and Simulation of All-Solid-State Three-Dimensional Li-Ion Batteries. *ACS Appl. Mater. Inter.* 8 (47), 32385–32391. doi:10.1021/acsami.6b12244

Tan, G., Wu, F., Lu, J., Chen, R., Li, L., and Amine, K. (2014). Controllable Crystalline Preferred Orientation in Li-Co-Ni-Mn Oxide Cathode Thin Films for All-Solid-State Lithium Batteries. *Nanoscale* 6 (18), 10611–10622. doi:10.1039/c4nr02949f

Teng, X., Qin, Y., Wang, X., Li, H., Shang, X., Fan, S., Li, Q., Xu, J., Cao, D., and Li, S. (2018). A Nanocrystalline Fe2O3 Film Anode Prepared by Pulsed Laser Deposition for Lithium-Ion Batteries. *Nanoscale Res. Lett.* 13. doi:10.1186/s11671-018-2475-8

Tintignac, S., Baddour-Hadjean, R., Pereira-Ramos, J. P., and Salot, R. (2014). High Rate Bias Sputtered LiCoO 2 Thinfilms as Positive Electrode for All-Solid-State Lithium Microbatteries. *Electrochimica Acta* 146, 472–476. doi:10.1016/j.electacta.2014.09.084

Varghese, A. P., Nair, S., and Santhanagopalan., D. (2019). Cobalt Oxide Thin Films for High Capacity and Stable Li-Ion Battery Anode. *J. Solid State. Electrochem.* 23 (2), 513–518. doi:10.1007/s10008-018-4158-x

Wang, X., and Yushin, G. (2015). Chemical Vapor Deposition and Atomic Layer Deposition for Advanced Lithium Ion Batteries and Supercapacitors. *Energy Environ. Sci.* 8 (7), 1889–1904. doi:10.1039/c5ee01254f

Wang, Z., Santhanagopalan, D., Zhang, W., Wang, F., Xin, H. L., He, K., Li, J., Dudney, N., and Meng, Y. S. (2016). *In Situ* STEM-EELS Observation of Nanoscale Interfacial Phenomena in All-Solid-State Batteries. *Nano Lett.* 16 (6), 3760–3767. doi:10.1021/acs.nanolett.6b01119

West, W. C., Whitacre, J. F., and Ratnakumar, B. V. (2003). Radio Frequency Magnetron-Sputtered LiCoPO[Sub 4] Cathodes for 4.8 V Thin-Film Batteries. *J. Electrochem. Soc.* 150 (12), A1660. doi:10.1149/1.1619987

Whitacre, J. F., West, W. C., and Ratnakumar, B. V. (2003). A Combinatorial Study of Li[sub y]Mn[sub x]Ni[sub 2−x]O[sub 4] Cathode Materials Using Microfabricated Solid-State Electrochemical Cells. *J. Electrochem. Soc.* 150 (12), A1676. doi:10.1149/1.1622957

Wise, A. M., Ban, C., Weker, J. N., Misra, S., Cavanagh, A. S., Wu, Z., Li, Z., Whittingham, M. S., Xu, K., George, S. M., and Toney, M. F. (2015). Effect of Al2O3 Coating on Stabilizing LiNi0.4Mn0.4Co0.2O2 Cathodes. *Chem. Mater.* 27 (17), 6146–6154. doi:10.1021/acs.chemmater.5b02952

Wu, J., Yuan, L., Zhang, W., Li, Z., Xie, X., and Huang, Y. (2021). Reducing the Thickness of Solid-State Electrolyte Membranes for High-Energy Lithium Batteries. *Energ. Environ. Sci.* 14 (1), 12–36. doi:10.1039/d0ee02241a

Xia, Q., Sun, S., Xu, J., Zan, F., Yue, J., Zhang, Q., Gu, L., and Xia, H. (2018). Self-Standing 3D Cathodes for All-Solid-State Thin Film Lithium Batteries with Improved Interface Kinetics. *Small*, 14 (52), 1804149. doi:10.1002/smll.201804149

Xia, Qiuying., Zhang, Q., Sun, S., Hussain, F., Zhang, C., Zhu, X., Meng, F., et al. (2020). Tunnel Intergrowth Li X MnO 2 Nanosheet Arrays as 3D Cathode for High-Performance All-Solid-State Thin Film Lithium Microbatteries, *Adv. Mater.*, 33(5), e2003524. doi:10.1002/adma.202003524

Xiao, C.-F., Kim, J. H., Cho, S.-H., Park, Y. C., Kim, M. J., Chung, K.-B., Yoon, S.-G., and Jung, J.-W. (2021). Ensemble Design of Electrode – Electrolyte Interfaces : Toward High-Performance Thin- Film All-Solid-State Li – Metal Batteries. *ACS Nano* 15 (3), 4561–4575. doi:10.1021/acsnano.0c08691

Xiao, D.-L., Tong, J., Feng, Y., Zhong, G.-H., Li, W.-J., and Yang, C.-L. (2018). Improved Performance of All-Solid-State Lithium Batteries Using LiPON Electrolyte Prepared with Li-Rich Sputtering Target. *Solid State Ionics* 324, 202–206. doi:10.1016/j.ssi.2018.07.011

Xie, J., Liao, L., Gong, Y., Li, Y., Shi, F., Pei, A., Sun, J., et al. (2017). Stitching H-BN by Atomic Layer Deposition of LiF as a Stable Interface for Lithium Metal Anode. *Sci. Adv.* 3 (11), 1–10. doi:10.1126/sciadv.aao3170

Xue, L., Zhang, Q., Zhu, X., Gu, L., Yue, J., Xia, Q., Xing, T., Chen, T., Yao, Y., and Xia, H. (2019). 3D LiCoO2 Nanosheets Assembled Nanorod Arrays via Confined Dissolution-Recrystallization for Advanced Aqueous Lithium-Ion Batteries. *Nano Energy* 56, 463–472. doi:10.1016/j.nanoen.2018.11.085

Yamada, I., Abe, T., Iriyama, Y., and Ogumi, Z. (2003). Lithium-Ion Transfer at LiMn2O4 Thin Film Electrode Prepared by Pulsed Laser Deposition. *Electrochemistry Commun.* 5 (6), 502–505. doi:10.1016/s1388-2481(03)00113-9

Yamada, I., Iriyama, Y., Abe, T., and Ogumi, Z. (2007). Lithium-Ion Transfer on a LixCoO2 Thin Film Electrode Prepared by Pulsed Laser Deposition-Effect of Orientation-. *J. Power Sourc.* 172 (2), 933–937. doi:10.1016/j.jpowsour.2007.05.072

Yoon, Y., Park, C., Kim, J., and Shin, D. (2013). The Mixed Former Effect in Lithium Borophosphate Oxynitride Thin Film Electrolytes for All-Solid-State Micro-batteries. *Electrochimica Acta* 111, 144–151. doi:10.1016/j.electacta.2013.08.053

Yu, X., Chen, X., Buchholz, D. B., Li, Q., Wu, J., Fenter, P. A., Bedzyk, M. J., Dravid, V. P., and Barnett, S. A. (2018). Pulsed Laser Deposition and Characterization of Heteroepitaxial LiMn2O4/La0.5Sr0.5CoO3 Bilayer Thin Films as Model Lithium Ion Battery Cathodes. *ACS Appl. Nano Mater.* 1 (2), 642–653. doi:10.1021/acsanm.7b00133

Yufit, V., Nathan, M., Golodnitsky, D., and Peled, E. (2003). Thin-Film Lithium and Lithium-Ion Batteries with Electrochemically Deposited Molybdenum Oxysulfide Cathodes. *J. Power Sourc.* 122 (2), 169–173. doi:10.1016/s0378-7753(03)00401-4

Conflict of Interest: Author ZB was employed by the Institute of Batteries LLC.

The remaining authors declare that the research was conducted in the absence of any commercial or financial relationships that could be construed as a potential conflict of interest.